1 **TITLE:**

2 ***In vivo* KRAS G12D/V degradation mediated by CANDDY using a modified**

3 **proteasome inhibitor**

4

5 **AUTHORS/AFFILIATIONS:**

6 **Satoshi Imanishi[1,#], Lijuan Huang[1,#], Shoko Itakura[2], Masamichi Ishizaka[1], Yoichi**

7 **Iwasaki[1], Tomohiro Yamaguchi[1], and Etsuko Miyamoto-Sato[1,2*]**

8 [1] Laboratory of Miyamoto-Sato Molecular Medical Sciences, Research Institute for

9 Science & Technology, Tokyo University of Science, 2641 Yamazaki, Noda, Chiba

10 278-0022, Japan

11 [2]Graduate School of Biological Sciences, Tokyo University of Science, 2641 Yamazaki,

12 Noda, Chiba 278-0022, Japan

13

14 [#]These authors contributed equally to this work.

15 [*] Correspondence: nekoneko@rs.tus.ac.jp

16

Summary

"Undruggable" proteins, such as RAS proteins, remain problematic despite efforts to discover inhibitors against them. KRAS mutants are prevalent in human cancers. Recently, the KRAS G12C inhibitor have been clinically approved, but inhibitors for KRAS G12D/V are still under development. Here, we described the development of a novel chemical knockdown strategy, termed CANDDY (Chemical knockdown with Affinity aNd Degradation DYnamics). This strategy involves a CANDDY tag modified from a proteasome inhibitor inducing direct proteasomal degradation. We constructed TUS-007 as a multispecific small molecule tethered from a KRAS interactor and CANDDY tag to target KRAS G12D/V. We confirmed that the degradation by TUS-007 was independent of target ubiquitination. This allows to solve a laborious design of matchmaker in the current ubiquitination-dependent proteolysis technology. And TUS-007 successfully suppressed tumors due to *in vivo* degradation of KRAS G12D/V. The CANDDY technology could represent a simple and rational strategy to degrade currently "undruggable" proteins.

Introduction

The majority (75%) of disease-causing proteins are "undruggable" (i.e., difficult to inhibit with small molecules). This difficulty reflects in the presence of smooth surfaces and lack of deep pockets, including proteins associated with cancer drivers and many interfaces for protein-protein interaction (PPI) (1, 2, 3). RAS family members (e.g., KRAS, HRAS, and NRAS) are most challenging to inhibit by small molecules (1, 4, 5, 6, 7). Mutations of KRAS, especially G12C, G12D, and G12V, are frequent in human cancers (7). The RAS protein activities depend on nucleotide loading in their GTP-binding pockets. The inhibition of this pocket has been attempted for nearly 40 years. However, progress has been hindered by the exceptionally high affinity between GTP and RAS proteins (1, 4, 8). While the inhibitor targeting KRAS G12C have been clinically approved recently (6, 9), inhibitors for KRAS G12D/V, which addresses greater clinical need, are still remained under development. These are important targets found in 95% of pancreatic cancers and 64% of colon cancers (7, 8). Inhibitors of the PPI between RAS and Son of Sevenless 1 (SOS1) (RAS-SOS inhibitor) have been investigated. Inhibitors that directly bind to RAS are not effective owing to their low

48 affinity (5). Thus, the current inhibition technologies are not enough to be effective for
49 undruggable proteins.
50 Pharmaceutical research on undruggable proteins, such as RAS, focuses on novel
51 modalities instead of inhibition (10, 11, 12). Proteolysis technologies, using
52 matchmakers between the target and E3 ligase or other ubiquitination related proteins
53 such as molecular chaperons for inducing target degradations, are expected to be
54 effective against undruggable proteins (13, 14, 15, 16, 17). However, matchmaker
55 design has been hampered by the dependency on target ubiquitination (16). It is difficult
56 to select a suitable E3 ligase for a target of interest because of limited knowledge about
57 the mechanism underlying substrate recognition by E3 ligases. Even if the target has an
58 established corresponding E3 ligase, there may be no available ligand for the E3 ligase.
59 Moreover, target ubiquitination may not always induce proteolysis, as in the case of
60 RAS, in which ubiquitination also regulates protein localization and activation (18).
61 Despite such difficulties, an effective inhibitor (9) was used recently for a proteolysis
62 inducer of KRAS G12C (19). However, no proteolysis inducer for KRAS G12D/V has
63 been reported. Current proteolysis technologies that depend on ubiquitination have

64 limited efficacy for undruggable targets (14). Therefore, to modulate diverse

65 undruggable targets, the difficulties in matchmaking should be eliminated (13).

66 Here, we report successful KRAS G12D/V degradation, mediated by a novel tool

67 named CANDDY (Chemical knockdown with Affinity aNd Degradation DYnamics).

68 This innovative approach induces direct proteasomal degradation (i.e., chemical

69 knockdown) of the target using a CANDDY tag derived from a proteasome inhibitor

70 that lacks the site for inhibitory activity (inhibitor site). By CANDDY technology,

71 chemical knockdown occurs without ubiquitination, so it can bypass the difficulties of

72 designing a matchmaker in current proteolysis techniques (13). Using an inefficient

73 target inhibitor, RAS/SOS inhibitor (5), we designed and synthesized a CANDDY

74 molecule called TUS-007 for KRAS G12D/V. We demonstrated KRAS G12D/V

75 chemical knockdown mediated by TUS-007 in cell-free, *in vitro*, and *in vivo* assays,

76 and *in vivo* tumor suppression.

77

78 **Results**

79 **A CANDDY molecule for targeting KRAS G12D/V proteins**

80 CANDDY molecules are bispecific molecules constructed from two modules;
81 a target interactor, which enables specific binding to the target, and a CANDDY tag,
82 which induces proteasomal degradation (Fig. 1a). The CANDDY tag is essential in
83 CANDDY technology and is a derivative lacking the inhibitor site of MLN2238 (MLN)
84 (20), a clinical proteasome inhibitor (Fig. 1b and Text S1.). To design TUS-007, we
85 employed a RAS-SOS inhibitor (5) (shown in Fig. 1c) which directly binds to KRAS
86 G12D, KRAS G12V, and wild-types of KRAS and HRAS as the target interactor
87 module. Since the binding to wild-type NRAS have not been reported, it was expected
88 to avoid the severe toxicity observed in a pan-RAS inhibitor (21). RAS-SOS inhibitor
89 was conjugated to the CANDDY tag using a NH_2 linker (Fig. 1c and Text S1.).
90 To compare the target binding of TUS-007 with that of the RAS-SOS
91 inhibitor, we performed a thermal shift assay. Unexpectedly, KRAS G12D/V proteins
92 incubated with TUS-007 were more resistant against heat treatment than those
93 incubated with RAS-SOS inhibitor (Fig. S1a). Alternatively, in a fluorescence-based
94 thermal shift assay, the T_m value of KRAS G12D incubated with TUS-007 was higher
95 than that of KRAS G12D incubated with RAS-SOS inhibitor (Fig. 1d and Fig. S1b).

96 These results suggest the higher affinity of TUS-007 to KRAS compared to RAS-SOS

97 inhibitor. In addition, we confirmed that TUS-007 had no inhibitory activity against the

98 catalytic β-subunits of proteasome (Fig. S2). This demonstrated that the CANDDY tag,

99 modified from a proteasome inhibitor, hardly inhibit proteasome activity.

100

101 **Chemical knockdown of KRAS G12D/V free from ubiquitination by TUS-007**

102 We attempted a chemical knockdown of KRAS G12D in the presence of 26S

103 proteasomes and in the absence of any ubiquitination related proteins in a cell-free

104 assay. Successful degradation was performed with 50% degradation concentration

105 (DC50) at 4 μM (Fig. 1e). The chemical knockdown mediated by TUS-007 was

106 counteracted by the presence of MLN (Fig. 1f). Additionally, RAS-SOS-NH_2 (a

107 synthetic intermediate without CANDDY tag, Fig. 1c) as a degradation-incompetent

108 control failed to induce the chemical knockdown (Fig. 1f), demonstrating CANDDY tag

109 is essential to induce the chemical knockdown. Although RAS-SOS inhibitor showed

110 80% inhibition of RAS-SOS PPI at 1 mM (5), DC80 of TUS-007 for KRAS G12D was

111 estimated as 16 μM (Fig. 1e). It implied that the conjugation with CANDDY tag

112 drastically improved the usefulness of RAS-SOS inhibitor. We also confirmed chemical

113 knockdown of KRAS G12V by TUS-007 in a cell-free assay in the absence of any

114 ubiquitination related proteins (Fig. S3). Furthermore, to obtain additional evidence of

115 degradation independent of ubiquitination, we co-treated HeLa cells expressing GFP-

116 KRAS G12D and DsRed with TUS-007 and MLN, E1 inhibitor (NAEi) or HSP70

117 inhibitor (VER-155008) (Fig. 2a). MLN counteracted the lowering of GFP signal

118 induced by TUS-007 treatment, but NAEi or VER-155008 did not. These results

119 demonstrated that chemical knockdown induced by TUS-007 was depend on

120 proteasome and independent of ubiquitination processes.

121

122 **TUS-007 induced targets-selective chemical knockdown *in vitro***

123 Using an *in vitro* assay, we then evaluated the chemical knockdown and

124 investigated the selectivity of TUS-007. We utilized RAS-less mouse embryonic

125 fibroblasts (MEFs) expressing human KRAS G12D, G12V, or G12C. These MEFs do

126 not proliferate in the absence of RAS (22). Immunoblotting analysis revealed that TUS-

127 007 induced the chemical knockdown of KRAS G12D/V, but not G12C, in RAS-less

128 MEFs (Fig. 2b). TUS-007 reduced the viability of RAS-less MEFs expressing KRAS
129 G12D/V but did not affect the viability of the cells expressing KRAS G12C (Fig. 2c),
130 confirming the selectivity of TUS-007 for KRAS G12D/V. We also assessed the
131 selectivity of TUS-007 for the human RAS family, including wild-type KRAS, HRAS,
132 and NRAS. TUS-007 did not affect the NRAS protein levels or the viability of RAS-
133 less MEFs expressing NRAS but affected KRAS or HRAS levels and the viability of
134 RAS-less MEFs expressing KRAS or HRAS (Fig. S4a and b). This result is consistent
135 with the previously reported data on the selectivity of the RAS-SOS inhibitor (5).
136 Therefore, it is expected not to induce intolerable toxicity previously observed with a
137 pan-RAS inhibitor *in vivo* (21) since TUS-007 is not a pan-RAS degrader. Furthermore,
138 the viability of RAS-less MEFs expressing KRAS G12C maintained even at 100 μM
139 TUS-007 (Fig. 2b and c), indicating that TUS-007 might have no remarkable off-target
140 toxicity in cell even at high concentrations. These results demonstrated the correlation
141 between the degradation of targets and the viability of cells by the concentrations of
142 TUS-007 without non-specific cytotoxic effect (Fig. 2b and c).
143

144 **The effects of TUS-007 on KRAS G12V-driven colon cancer**

145 Approximately 64% of human colon cancers reportedly express KRAS

146 mutants. KRAS G12V is found in nearly half of the patients and is correlated with poor

147 prognosis (8). Therefore, we investigated whether TUS-007 can suppress the growth of

148 human KRAS G12V-driven colon cancer cells. We conducted an experiment with the

149 SW620-Luc KRAS G12V homozygous human colon cancer cell line (23). TUS-007

150 induced chemical knockdown of KRAS (Fig. 3a), accompanied by an increase in the

151 annexin V-positive fraction in SW620-Luc cells (Fig. 3b and Fig. S5). However, RAS-

152 SOS-NH_2 and cetuximab did not induce apoptosis (Fig. 3b and Fig. S5). In contrast,

153 treatment with TUS-007 did not result in significant changes in the annexin V-positive

154 fraction in HT29-Luc RAS-independent colon cancer cells (Fig. 3c and Fig. S6).

155 Alternatively, the apoptosis induction in SW620-Luc cells was confirmed by caspase

156 3/7 activation (Fig. 3d). Importantly, TUS-007 induced the apoptosis in SW620-Luc

157 cells at the same concentration at which the chemical knockdown of KRAS was

158 significant (Fig. 3a, b and Fig. S7). These findings indicated that TUS-007 selectively

159 induces apoptosis in SW620-Luc cells by chemical knockdown of KRAS G12V *in*

160 *vitro*.

161 Next, to assess the effectiveness of TUS-007 *in vivo*, we transplanted SW620-

162 Luc cells subcutaneously in immunodeficient mice. TUS-007 or cetuximab was

163 administered to the xenograft mice by intraperitoneal (i.p.) injection. TUS-007

164 significantly attenuated tumor progression (Fig. 3e, f and Fig. S8a) and induced KRAS

165 G12V chemical knockdown in tumors (Fig. S8b). The body weights of the mice were

166 not affected by TUS-007 treatment (Fig. S8c). These results suggested that TUS-007 is

167 effective *in vivo* against KRAS G12V-driven tumors.

168

169 **The effects of TUS-007 on KRAS G12D-driven pancreatic cancer**

170 Approximately 95% of pancreatic cancers harbor KRAS mutations, and the

171 G12D mutation is particularly prevalent and strongly correlated with poor prognosis (8).

172 Therefore, we examined the effects of TUS-007 in human pancreatic cancer cell lines.

173 As expected, TUS-007 degraded the KRAS protein (Fig. 4a) and induced apoptosis

174 (Fig. 4b) in SW1990 KRAS G12D-driven pancreatic cancer cells (24). The apoptosis

175 induction in SW1990 cells was approximately correlated with concentrations of

176 chemical knockdown of KRAS (Fig. 4a and b). The correlation between the

177 concentration of apoptosis induction and degradation induction was further confirmed

178 (Fig. S9). In addition, apoptosis was induced with caspase 3/7 activation in SW1990

179 cells (Fig. 4c), which was counteracted by a proteasome inhibitor MLN but not by a

180 ubiquitination inhibitor NAEi (Fig. 4d). Therefore, it suggested that TUS-007 induced

181 apoptosis owing to target degradation independent of ubiquitination.

182 In mice with SW1990 cells implanted subcutaneously, the oral (per os; p.o.)

183 administration of TUS-007 significantly suppressed the tumor growth (Fig. 4e) and

184 reduced tumor weight (Fig. S10a). The i.p. injection of TUS-007 also suppressed

185 subcutaneously implanted tumor growth in mice (Fig. S10b). Both p.o. (Fig. 4f) and i.p.

186 (Fig. S10c) administrations showed no change in body weight. Here, we examined the

187 chemical knockdown of KRAS, HRAS and NRAS with TUS-007 in pancreas from the

188 identical mice used in Fig. 4e and f. In accordant with the results in RAS-less MEFs,

189 TUS-007 induced the degradation of KRAS and HRAS but not NRAS (Fig. S11). Thus,

190 there was no sign of toxicity such as body weight losses in contrast to a pan-RAS

191 inhibitor (21).

192 Moreover, extracellular signal-regulate kinase (ERK) and protein kinase B

193 (AKT) phosphorylation were decreased in tumor by both p.o. and i.p. administrations

194 (Fig. S12a and b), indicating that both RAS-mitogen-activation protein (RAS-MAP)

195 and RAS- phosphoinositide 3-kinase (RAS-PI3K) signaling were inhibited. It is

196 difficult for inhibitors to inhibit both RAS-MAP and RAS-PI3K signaling, even using a

197 clinically effective KRAS G12C inhibitor (6). Thus, the chemical knockdown of KRAS

198 by CANDDY might offer a clinical benefit. Taken together, these results indicated that

199 TUS-007 exerted *in vivo* antitumor activity *via* the chemical knockdown of KRAS

200 G12D/V and suppression of KRAS signaling.

201

202 **TUS-007 exerted anti-tumor activity even in orthotopic xenograft model mice**

203 SW1990-Luc cells were transplanted directly into the pancreas of mice as an

204 orthotopic xenograft model. The mice were subsequently treated p.o. with TUS-007.

205 Remarkably, *in vivo* imaging revealed reductions in tumor growth (Fig. 5a, b and Fig.

206 S13a) and tumor weight (Fig. S13b). Results from immunohistochemical analysis (Fig.

207 5c left panels and Fig. S13c left bar graph) and immunoblotting (Fig. 5d) confirmed the

208 chemical knockdown of KRAS G12D in the tumor tissues of mice treated with TUS-

209 007. Furthermore, higher concentrations of positive cells were observed in the terminal

210 deoxynucleotidyl transferase dUTP nick-end labeling (TUNEL) assay in the tumor

211 tissues of TUS-007-treated mice, implying the induction of apoptosis in the TUS-007-

212 treated tumors (Fig. 5c right panels and Fig. S13c right bar graph). The body weights of

213 the orthotopic xenograft model mice were not affected by TUS-007 (Fig. S13d).

214 Overall, these results demonstrated that oral treatment with TUS-007 induces KRAS

215 G12D chemical knockdown and suppresses pancreatic tumor growth without the sign of

216 weight loss and significant toxicity in the orthotopic xenograft model.

217 Finally, we examined the *in vivo* concentrations of TUS-007. When an i.p

218 dose of 80 mg/kg TUS-007 was administered to healthy mice, a concentration (45

219 ng/mg, equivalent to 53 μM) of TUS-007 was observed in the pancreas (Table S1.).

220 This TUS-007 concentration *in vivo* agreed with the concentration at which chemical

221 knockdown and apoptotic indicators were observed in SW1990 cells *in vitro* (Fig. 4a-c).

222 Therefore, these results suggest that there is no contradiction between our *in vivo* and *in*

223 *vitro* results.

224

225 **CANDDY applied to another undruggable target**

226 To evaluate the versatility of CANDDY approach, we designed a CANDDY

227 molecule targeting MDM2 (MDM2-CANDDY), a negative regulator of P53, using a

228 P53-MDM2 PPI inhibitor with a weak potency (25) as an interactor module of a

229 CANDDY molecule (Fig. S14a and Text S1.). MDM2-CANDDY successfully induced

230 the chemical knockdown of MDM2 in HCT-116 human colon cancer cells (Fig. S14b).

231 P53-MDM2 PPI is still well-recognized "undruggable" target (26). This result

232 suggested the potential versatility of CANDDY to target other undruggable proteins.

233

234 **Discussion**

235 We provided the proof of concept that CANDDY tag enabled to induce

236 proteasomal degradation through ubiquitination-independent process (Fig. 1f and Fig.

237 2a) in this report. Considering the proteasome enable to degrade any targets, the

238 CANDDY tag modified from a proteasome inhibitor (Fig. 1b) can eliminate the
239 difficulties of matchmaking of targets and specific ubiquitination related proteins such
240 as E3 ligases in current protein degradation (13, 14). Thus, CANDDY technology could
241 provide a simple and rational approach to induce the chemical knockdown of currently
242 undruggable targets because of the CANDDY tag independent of ubiquitination.
243 Expectedly, we confirmed the correlations between degradation of KRAS
244 G12D and V and apoptosis in pancreatic and colon cancer cells, respectively (Fig. 3a, b,
245 Fig. 4a-d, Fig. S7 and S9), and *in vivo* (Fig. 5c and Fig. S13c). Both *in vitro* and *in vivo*,
246 TUS-007 achieved efficacy mediated by moderate degradations of KRAS G12D/V. A
247 previous study showed that the moderate decrease of KRAS protein is enough to inhibit
248 tumor growth *via* more strong inhibition of downstream signal (12) as well as we
249 showed (Fig. S12). Thus, *in vitro* and *in vivo* results could be reasonable. Importantly,
250 the concentration of TUS-007 in pancreas agreed with the effective concentration *in*
251 *vitro* (Table S1.), demonstrating the consistency between our *in vivo* and *in vitro* results.
252 On the other hand, the requirement of high concentrations generally raises concerns
253 about toxicity. However, TUS-007 did not show non-specific cytotoxicity *in vitro* even

254 at high concentration (Fig. 2c) and no sign of body weight losses was observed in TUS-
255 007 treated mice (Fig. 4f, Fig. S8c, S10c and S13d) in contrast to a pan-RAS inhibitor
256 (21). These results suggest that TUS-007 induced *in vivo* degradation of KRAS
257 G12D/V resulting in suppression of colon and pancreatic tumors without no significant
258 toxicity even at high concentrations.

259 No effective drug to inhibit or degrade KRAS G12D/V has been reported yet.
260 Also, the proteolysis field does not still have enough evidence that can target and
261 degrade tough and valuable undruggable proteins (14). Of note, in spite of a poor
262 inhibitor was employed as interactor, TUS-007 induced chemical knockdown of KRAS
263 G12D/V *in vivo*, resulting in suppression of a pancreatic tumor even in the orthotopic
264 xenograft model with oral administrations (Fig. 5). In addition, another weak inhibitor
265 of PPI, P53-MDM2 PPI inhibitor (25) (Fig. S14), was useful as the interactor of
266 CANDDY molecules. Thus, CANDDY technology could be expectedly applied to
267 tough and valuable undruggable targets still remaining with no effective inhibitors. In
268 the future, CANDDY has the potential to overcome the current limitations of

269 proteolysis and to expand the application scope of degraders for molecular targeting

270 therapy of aggressive and deadly diseases caused by undruggable targets.

271

272

273 **References**

274 1. Khan, I., Rhett, J. M. & O'Bryan, J. P. Therapeutic targeting of RAS: New Hope for

275 drugging the "undruggable". *Biochim. Biophys. Acta Mol. Cell Res.* **1867**, 118570

276 (2020).

277 2. Fujimori, S., et al. Next-generation sequencing coupled with a cell-free display

278 technology for high-throughput production of reliable interactome data. *Sci. Rep.* **2,**

279 691 (2012).

280 3. Scott, D. E., Bayly, A. R., Abell, C. & Skidmore, J. Small molecules, big targets:

281 Drug discovery faces the protein-protein interaction challenge. *Nat. Rev. Drug*

282 *Discov.* **15,** 533–550 (2016).

283 4. Stephen, A. G., Esposito, D., Bagni, R. K. & McCormick, F. Dragging Ras back in

284 the ring. *Cancer Cell* **25,** 272–281 (2014).

285 5. Sun, Q., et al. Discovery of small molecules that bind to K-Ras and inhibit Sos-

286 mediated activation. *Angew. Chem. Int. Ed.* **51,** 6140–6143 (2012).

287 6. Canon, J., et al. The clinical KRAS(G12C) inhibitor AMG 510 drives anti-tumour

288 immunity. *Nature* **575,** 217–223 (2019).

289 7. Hobbs, G. A., Der, C. J. & Rossman, K. L. RAS isoforms and mutations in cancer at
290 a glance. *J. Cell Sci.* **129,** 1287–1292 (2016).
291 8. Haigis, K. M. KRAS alleles: The devil is in the detail. *Trends Cancer* **3,** 686–697
292 (2017).
293 9. Sheridan, C. Grail of RAS cancer drugs within reach. *Nat. Biotechnol.* **38,** 6–8
294 (2020).
295 10. Shin, S. M., et al. Antibody targeting intracellular oncogenic Ras mutants exerts
296 anti-tumour effects after systemic administration. *Nat. Commun.* **8,** 15090 (2017).
297 11. Yin, W. & Rogge, M. Targeting RNA: A transformative therapeutic strategy. *Clin.*
298 *Transl. Sci.* **12,** 98–112 (2019).
299 12. Ross, S. J., et al. Targeting KRAS-dependent tumors with AZD4785, a high-affinity
300 therapeutic antisense oligonucleotide inhibitor of KRAS. *Sci. Transl. Med.* **9,** pii:
301 eaal5253. doi: 10.1126/scitranslmed.aal5253 (2017).
302 13. Deshaies, R. J. Multispecific drugs herald a new era of biopharmaceutical
303 innovation. *Nature* **580,** 329–338 (2020).

304 14. Scudellari, M. Protein-slaying drugs could be the next blockbuster therapies. *Nature*
305 **567,** 298–300 (2019).
306 15. Cromm, P. M. & Crews, C. M. Targeted protein degradation: From chemical
307 biology to drug discovery. *Cell Chem. Biol.* **24,** 1181–1190 (2017).
308 16. Pettersson, M. & Crews, C. M. PROteolysis TArgeting Chimeras (PROTACs) -
309 Past, present and future. *Drug Discov. Today Technol.* **31,** 15–27 (2019).
310 17. Churcher, I. Protac-induced protein degradation in drug discovery: Breaking the
311 rules or just making new ones? *J. Med. Chem.* **61,** 444–452 (2018).
312 18. Dohlman, H. G. & Campbell, S. L. Regulation of large and small G proteins by
313 ubiquitination. *J. Biol. Chem.* **294,** 18613–18623 (2019).
314 19. Bond, M. J., et al. Targeted degradation of oncogenic KRASG12C by VHL-
315 recruiting PROTACs. *ACS Cent. Sci.* **6**, 1367–1375 (2020).
316 20. Kisselev, A. F., van der Linden, W. A. & Overkleeft, H. S. Proteasome inhibitors:
317 An expanding army attacking a unique target. *Chem. Biol.* **19,** 99–115 (2012).
318 21. Welsch, M. E., et al. Multivalent small-molecule pan-RAS inhibitors. *Cell* **168,**
319 878–889.e29 (2017).

320 22. Drosten, M., et al. Genetic analysis of Ras signaling pathways in cell proliferation,
321 migration and survival. *EMBO J.* **29,** 1091–1104 (2010).
322 23. Ahmed, D., et al. Epigenetic and genetic features of 24 colon cancer cell lines.
323 *Oncogenesis* **2,** e71 (2013).
324 24. Jansen, J. M., et al. Inhibition of prenylated KRAS in a lipid environment. *PLOS*
325 *ONE* **12,** e0174706 (2017).
326 25. Kumar, S. K., et al. Design, synthesis, and evaluation of novel boronic-Chalcone
327 derivatives as antitumor agents. *J. Med. Chem.* **46**, 2813–2815 (2003).
328 26. Shangary, S. & Wang, S. Targeting the MDM2-p53 Interaction for Cancer Therapy.
329 *Clin. Cancer. Res.* **14,** 5318–5324 (2008).
330 27. Scott, D. E., Bin, Y. & Charlene F. Proteolysis targeting chimeras (PROTACs) in
331 'beyond rule-of-five' chemical space: Recent progress and future challenges, *Bioorg*
332 *Med Chem Lett*, **29**, 1555–1564 (2019).
333

334 **Data availability**

335 Source data are provided for all experiments. Other data that support the

336 findings of this study are available from the corresponding author, upon reasonable

337 request.

338

339 **Acknowledgments** We thank Masaaki Ozawa, Mai Hasegawa, Takuya Yogi, Mizuki

340 Kanazawa, and Sachi Tsuji for help with the *in vitro* studies, Yuri Sato for help with the

341 *in vivo* studies, Megumi Tsukamoto and Megumi Saito for help with both *in vitro* and *in*

342 *vivo* studies. We thank the NCI RAS initiative for providing the RAS-less MEFs used

343 in this work, the Uchiro Laboratory for performing the high-resolution mass

344 spectrometry analysis at the Research Equipment Center (Tokyo University of Science

345 (TUS), Japan), the Gunji Laboratory (TUS) for the use of their high-performance liquid

346 chromatography instruments, the Iwakura and Abe Laboratories in the animal facility of

347 the Research Institute for Biomedical Sciences (TUS) for maintaining the mice, Fumito

348 Ishizuka and Naoki Takeda (NARD Institute, Ltd.) for contributions to the chemical

349 synthesis, and Hiroyuki Ohashi for the helpful suggestions. This work was financially

supported by the Program for Creating STart-ups from Advanced Research and Technology (START Program: 962238), and the joint research with FuturedMe Inc.

Author contributions S. Im., L. H., S. It., and E. M. S. designed the study. S. Im., L. H., S. It., M. I. and T. Y. performed the *in vitro* and *in vivo* experiments. Y. I. performed chemical analyses. E. M. S. supervised the study. All authors discussed the study and approved the submitted manuscript.

Competing interests The authors declare no competing interests.

Text S1. is available in the online version of the paper.

363 **Figure legends**

364

365 **Fig. 1. RAS chemical knockdown *in vitro*.**

366 **a,** Principle of the CANDDY technology. Each CANDDY molecule includes a target

367 interactor (burgundy hexagon) and a CANDDY tag (yellow oval). The target protein is

368 bound by the CANDDY molecule *via* the target interactor and is directly degraded by

369 proteasome via the CANDDY tag. **b,** The CANDDY tag was synthesized by chemically

370 inactivating the inhibitor site of MLM2238 (MLN). **c,** Structures of the RAS-SOS

371 inhibitor (ref. 5), RAS-SOS-NH_2, and TUS-007. **d,** KRAS G12D was mixed with

372 DMSO, RAS-SOS inhibitor (4 mM) or TUS-007 (4 mM) and incubated under heating

373 from 25 °C to 99 °C. The denature of KRAS G12D was monitored by the fluorescence.

374 The typical curve of each group was shown. **e,** The correlation between relative amount

375 of KRAS G12D and concentration of TUS-007 were approximated with Rodbard using

376 the means of 3 independent examinations. The DC50 was estimated about 4 μM. **f,**

377 TUS-007 induced KRAS G12D chemical knockdown by 26S proteasome in a cell free

378 assay. KRAS G12D was incubated with 26S proteasome and agents as indicated for 3 h.

379 **Fig. 2. RAS chemical knockdown in cells.**

380 **a,** TUS-007 induced chemical knockdown was independent of ubiquitination. GFP

381 fused KRAS G12D and DsRed were transiently expressed in HeLa cells. The cells were

382 treated with TUS-007 in the presence of a proteasome inhibitor (MLN), a ubiquitination

383 inhibitor (NAEi) and a molecular chaperon inhibitor (HSP70 inhibitor: VER-155008)

384 for 24 h. **b & c,** RAS-less MEFs expressing KRAS G12D, G12V or G12C were

385 incubated with TUS-007 for 72 h. Representative blots of KRAS are shown (b). The

386 relative amounts of KRAS mutants normalized to GAPDH are shown in the bar graph

387 (mean ± SEM; n = 3–4). The cell viability was also measured (mean ± SEM; n = 3–4)

388 (g). *P < 0.05 and ** P < 0.01 vs. DMSO. TUS-007 induced chemical knockdown did

389 not cause non-specific cytotoxicity.

390

391 **Fig. 3. Chemical knockdown and tumor suppression *in vitro* and *in vivo* in KRAS**

392 **G12V-driven human colon cancer cells by TUS-007 treatment.**

393 **a,** Immunoblotting analysis of KRAS G12V chemical knockdown in SW620-Luc cells

394 treated with TUS-007 for 48 h at the indicated doses. The KRAS band intensity was

395 normalized to that of GAPDH (mean ± SEM; n = 3). *P < 0.05 and **P < 0.01 vs.

396 DMSO. **b & c,** The ratio of apoptotic cells were analyzed in colon cancer SW620-Luc

397 cells (**b**) and HT29-Luc cells (**c**), a KRAS-independent, BRAF-dependent cell line (Ctx

398 + Vem: 100 mg/ml cetuximab and 40 mM vemurafenib). Cells were treated with each

399 compound for 48 h in terms of the number of annexin V-positive/PI-negative apoptotic

400 cells detected by flow cytometry (mean ± SEM; n = 2–5). **P < 0.01, and ***P < 0.001

401 vs. DMSO. **d,** Relative activity of caspase 3/7 in SW620-Luc cells treated with TUS-

402 007 or 5-fluorouracil (5-FU) for 48 h (mean ± SEM; n = 3). *P < 0.05 and **P < 0.01

403 vs. DMSO. **e,** Tumor volume in mice with SW620-Luc cells transplanted

404 subcutaneously and treated with i.p. administration every 3 days (mean ± SEM; n = 6–

405 8). *P < 0.05 vs. vehicle alone. **f,** Tumors of SW620-Luc cells at day 21 from the same

406 mice shown in **e** (n = 6–8).

407

408 **Fig. 4. Chemical knockdown and tumor suppression *in vitro* and *in vivo* in KRAS**

409 **G12D-driven human pancreatic cancer cells by TUS-007 treatment.**

410 **a,** KRAS G12D chemical knockdown induced by TUS-007 in SW1990 cells. SW1990

411 cells were treated with TUS-007 for 72 h and analyzed by immunoblotting. The KRAS

412 G12D band intensity was normalized to that of GAPDH (mean ± SEM; n = 4). *P <

413 0.05 vs. DMSO. **b,** The proportion of annexin V-positive apoptotic SW1990 cells

414 treated with DMSO, RAS-SOS-NH_2 or TUS-007 for 72 h (mean ± SEM; n = 3). *P <

415 0.05 vs. DMSO or RAS-SOS-NH_2. **c,** TUS-007 increased the caspase 3/7 activity in

416 SW1990 cells after treatment for 96 h (mean ± SEM; n = 3). *P < 0.05 and **P < 0.01

417 vs. DMSO. **d,** Caspase 3/7 activation by TUS-007 was proteasome dependent and

418 ubiquitination independent. SW1990 cells were treated with the agents for 96 h (mean ±

419 SEM; n = 3). **P < 0.01 vs. DMSO, ##P < 0.01 vs. TUS-007 (100 μM) only, and †no

420 statistically significant difference compared with TUS-007 (100 μM) only. **e,** Tumor

421 volume in mice with SW1990 cells transplanted subcutaneously and treated with p.o.

422 administered TUS-007 or vehicle (mean ± SEM; n = 6–9). The agents were

423 administered every 3 days. **P < 0.01 vs. vehicle alone. **f,** Body weight changes in

424 mice with SW1990 cells transplanted subcutaneously (mean ± SEM; n = 6–9).

425

426 **Fig. 5. TUS-007 suppresses the growth of KRAS G12D-positive orthotopic**

427 **pancreatic tumors.**

428 **a,** Images showing the luciferase activity and total flux in orthotopic tumors

429 transplanted SW1990-Luc cells *in vivo*. **b,** Tumor growth (bioluminescence) in identical

430 mice treated with vehicle or TUS-007 administered p.o. every 3 days. (mean ± SEM; n

431 = 6). *P < 0.05 vs. vehicle alone. **c,** Representative histochemical staining of KRAS and

432 TUNEL in orthotopic tumor sections from the same mice used in **a**. The scale bar is 60

433 μm. **d,** Immunoblotting of KRAS G12D in tumor lysates from the same mice used in **a**.

434 The bar graph shows quantification of KRAS G12D normalized to GAPDH (mean ±

435 SEM; n = 6). **P < 0.01 vs. vehicle alone.

436

437 **Fig. S1. The heat resistance of KRAS G12D/V incubated with TUS-007.**

438 **a,** Evaluation of the target-binding affinity of TUS-007 to KRAS mutants by a thermal

439 shift assay. Recombinant KRAS was treated with the vehicle, RAS-SOS inhibitor, or

440 TUS-007 for 30 min, heated at the indicated temperature for 20 min, then analyzed by

441 immunoblotting. **b,** The means of T_m values from fluorescence-based thermal shift

442 assay shown in Fig. 1d. (mean ± SEM; n = 2). *P < 0.05 vs. DMSO, #P < 0.05 vs. RAS-

443 SOS inhibitor.

444

445 **Fig. S2. Effects of TUS-007 on proteasome activity levels.**

446 The levels of chymotrypsin-like (β5), trypsin-like (β2), and caspase-like (β1)

447 proteasome activities was monitored by Suc-LLVY-AMC, Bz-VGR-AMC, and Z-LLE-

448 AMC, respectively. AMC fluorescence was monitored by a plate reader with excitation

449 and emission filters of 360 and 460 nm, respectively (DMSO, 30 min = 1) (mean ±

450 SEM; n = 2–3).

451

452 **Fig. S3. TUS-007 induced degradation of KRAS G12V in cell free assay.**

453 Successful KRAS G12V degradation by TUS-007. KRAS G12V protein was incubated

454 with TUS-007 at the indicated concentrations in the presence of 26S proteasome for 1 h

455 (mean ± SEM; n = 3). *P < 0.05 vs. DMSO.

456

457 **Fig. S4. Selective chemical knockdown of RAS variants in RAS-less MEFs**

458 **expressing different types of human RAS.**

459 **a,** Relative viability of RAS-less MEFs expressing WT human RAS family members

460 after incubation with TUS-007 or DMSO. (mean ± SEM; n = 3–5). *P < 0.05 and **P <

461 0.01 vs. DMSO. **b,** Degradation of WT human RAS family members in RAS-less MEFs

462 treated with TUS-007 or DMSO for 72 h (mean ± SEM; n = 4–5). *P < 0.05 and **P <

463 0.01 vs. DMSO.

464

465 **Fig. S5. FACS plots for Annexin V- PI staining of SW620-Luc cells.**

466 SW620-Luc cells were treated with the indicated agents for 48 h, followed by staining

467 with Annexin V-FITC and PI. The typical plots are shown.

468

469 **Fig. S6. FACS plots for Annexin V- PI staining of HT29-Luc cells.**

470 HT29-Luc cells were treated with the indicated agents for 48 h, followed by staining

471 with Annexin V-FITC and PI. The typical plots are shown.

472

473 **Fig. S7. TUS-007 induced apoptosis only when KRAS degradation was detected in**

474 **KRAS G12V driven cancer cells.**

475 SW620-Luc cells were treated with TUS-007 for 12 h (mean ± SEM; n = 3). The left

476 axis indicates KRAS/GAPDH, and the right axis indicates relative ratio of apoptotic

477 cells. *P < 0.05 vs. DMSO. The ratio of KRAS/GAPDH was determined by image

478 analyses of immunoblotting and ration of apoptotic cells were measured using FACS.

479

480 **Fig. S8. Effects of TUS-007 on the growth of colon cancer subcutaneous xenografts**

481 **and toxicity.**

482 **a,** Comparison of SW620-Luc tumor weight at 21 days after injection (mean ± SEM; n

483 = 6–8). *P < 0.05 vs. vehicle alone. **b,** Immunoblotting of KRAS G12V chemical

484 knockdown in tumors from the same mice used in Fig. 2e (mean ± SEM; n = 6). **P <

485 0.01 vs. vehicle alone. **c,** Body weight changes in mice with SW620-Luc cells

486 transplanted subcutaneously (mean ± SEM; n = 6–8).

487

488 **Fig. S9. TUS-007 induced apoptosis only when KRAS degradation was detected in**

489 **KRAS G12D driven cancer cells.**

490 SW1990 cell were treated with TUS-007 for 12 h (mean ± SEM; n = 3). The left axis

491 indicates KRAS/GAPDH, and the right axis indicates relative ratio of apoptotic cells.

492 *P < 0.05 vs. DMSO. The ratio of KRAS/GAPDH was determined by image analyses

493 of immunoblotting and ration of apoptotic cells were measured using FACS.

494

495 **Fig. S10. Effects of TUS-007 on the growth of pancreatic cancer subcutaneous**

496 **xenografts and toxicity.**

497 **a,** Tumors of SW1990 cells from the same mice shown and comparison of tumor weight

498 in Fig. 3e at 21 days after p.o. administration (mean ± SEM; n = 6–9). *P < 0.05 vs.

499 vehicle alone. **b,** Tumor volume in mice with SW1990 cells transplanted

500 subcutaneously and treated with i.p. administered TUS-007 or vehicle (mean ± SEM; n

501 = 6–9). The agents were administered every three days. *P < 0.05 vs. vehicle. **c,** Body

502 weight changes in mice with SW1990 cells transplanted subcutaneously (mean ± SEM;

503 n = 6–9).

504

505 **Fig. S11. Effects of oral treatment with TUS-007 on wild type RAS in pancreas.**

506 The immunoblotting analyses of wt RAS proteins in pancreas from the same mice

507 shown in Fig. 3e (mean ± SEM; n = 6–9). *P < 0.05 vs. vehicle alone.

508

509 **Fig. S12. Effect of TUS-007 on RAS signaling in pancreatic cancer subcutaneous**

510 **xenografts.**

511 Immunoblotting of KRAS and downstream signaling molecules in tumors from the

512 same mice used in Fig. 3e (**a**: p.o. treatment) and Fig. S. 10c (**b**: i.p. treatment). The

513 quantitative analysis of the immunoblotting was shown as bar graph, where the KRAS

514 values were normalized to GAPDH, the p-ERK values were normalized to the total

515 ERK, and the p-AKT values were normalized to the total AKT (mean ± SEM; n = 6).

516 *P < 0.05 vs. vehicle.

517

518 **Fig. S13. Effect of TUS-007 on growth of orthotopic pancreatic cancer xenografts**

519 **expressing mutant KRAS.**

520 **a,** Tumor growth, as assessed by luciferase signal, in individual mice orthotopically

521 transplanted SW1990-Luc cells treated with TUS-007 (orange) or vehicle alone (blue)

522 (mean ± SEM; n = 6). **b,** Pancreases from orthotopic xenograft model mice at day 21

523 after treatment with TUS-007 (lower-left panel) or the vehicle alone (upper-left panel)

524 and comparison of their weights (right graph) (mean ± SEM; n = 6). *P < 0.05 vs.

525 vehicle alone. **c,** The quantitative analyses of the KRAS G12D-positive area (left) and

526 TUNEL-positive area (right) in Fig. 4c (mean ± SEM; n = 6). **P < 0.01 vs. vehicle

527 alone. **d,** Body weight changes in mice subjected to orthotopic transplantation of

528 SW1990-Luc cells (mean ± SEM; n = 6).

529

530 **Fig. S14. CANDDY induced degradation of MDM2, a common undruggable**

531 **target.**

532 **a,** The structure of MDM2-CANDDY using P53-MDM2 PPI inhibitor, with IC50 value

533 between 6-25 μM. **b,** MDM2-CANDDY degraded MDM2 in the dose dependent

534 manner. The human colon cancer cells HCT-116 were incubated for 48 h with MDM2-

535 CANDDY (mean ± SEM; n = 3). **P < 0.01 vs. DMSO.

536

537 **Table S1. The concentration of TUS-007 in pancreas was maintained for 72 h.**

538 The concentration of TUS-007 in pancreas from healthy wild-type mice i.p. treated with

539 TUS-007 at 80 mg/kg (means ± SEM; n = 5). The samples were obtained at indicated

540 time points after i.p. injection. The concentration of TUS-007 was measured with

541 HPLC.

542

543

544 **STAR Methods**

545

546 **Cell lines.** SW1990 and HCT-116 cells were purchased from the American Type

547 Culture Collection (Manassas, VA, USA). SW620-Luc and HT29-Luc cells were

548 purchased from the National Institute of Biomedical Innovation, Health, and Nutrition

549 (Osaka, Japan). RAS-less MEF cell lines (wild-type (wt) KRAS, KRAS G12D, KRAS

550 G12V, KRAS G12C, NRAS and HRAS) were obtained from the National Institutes of

551 Health (NCI RAS Initiative at the Frederick National Laboratory for Cancer Research,

552 Frederick, MD, USA).

553

554 **Animal studies.** BALB/cA-nu/nu and BALB/cA (female, 7-9 weeks old) were

555 purchased from CLEA Japan (Tokyo, Japan). The animals were maintained in

556 conventional housing conditions, with a daily 12-h light/dark cycle, and given food and

557 water *ad libitum*. The animals were cared for in accordance with the NIH Guide for the

558 Care and Use of Laboratory Animals. All animal experiments were approved by the

559 Committee on Animal Experimentation of the Tokyo University of Science.

560

561 **Reagents.** MLN2238 (A10600) was purchased from AdooQ BioScience (Irvine, CA,

562 USA). NAEi was purchased from AdipoGen (San Diego, CA, USA). Human 26S

563 Proteasome Protein (E-365) and Human 20S Proteasome Protein (E-360) were

564 purchased from R&D Systems (Minneapolis, MN, USA). Human KRAS (G12D) and

565 the corresponding His tag (12259-H07E1) were purchased from Sino Biological

566 (Beijing, China). Human KRAS (G12V), 2-186, and the corresponding His tag (R06-

567 32BH) were obtained from SignalChem Lifesciences (Richmond, British Columbia,

568 Canada).

569

570 **Measurement of 20S proteasome activity.** The chymotrypsin-like (β5), trypsin-like

571 (β2), and caspase-like (β1) activities of the 20S proteasome were measured using a 20S

572 Proteasome Activity Kit GOLD (StressMarq Bioscience Inc., Victoria, British

573 Columbia, Canada). Purified 20S proteasome (0.1 μg) was incubated in the presence of

574 CANDDY molecules (1, 4, 10, 20, 40, 80, and 160 μM) or MLN2238 at the indicated

575 concentrations for 30 min at room temperature. After incubation, 100 mM of

576 fluorogenic peptide substrates, Suc-LLVY-AMC (β5 substrate), Bz-VGR-AMC (β2

577 substrate), or Z-LLE-AMC (β1 substrate), was added, followed by incubation for 1 h at

578 room temperature. The reaction mixture was then transferred to a 96-well plate, and the

579 fluorecence from hydrolyzed AMC groups was measured using a Synergy HT multi-

580 channel microplate reader (BioTek Instruments, Inc., Winooski, VT, USA) with a 360

581 nm excitation filter and 460 nm emission filter.

582

583 **Evaluation of affinity of TUS-007 for KRAS in a thermal shift assay.** The KRAS

584 G12D/V (100 nM) was preincubated with TUS-007, a RAS-SOS inhibitor, or 10%

585 DMSO in 75 mM phosphate buffer (pH 7.5) for 30 min at 37 °C (G12D) or for 20 min

586 at 25 °C (G12V). Aliquots of the reaction solution were sampled into separate

587 microtubes and heated for 30 min at 70, 80, or 90 °C for G12D, or at 40, 50, or 60 °C

588 for G12V. After centrifugation at 18,000 ×*g* for 20 min, the supernatants were analyzed

589 by SDS-PAGE, followed by immunoblotting using an anti-KRAS antibody (1:1000,

590 WH0003845MI, Sigma-Aldrich, St. Louis, MO, USA). Immunoreactive bands were

591 detected using an iBright CL1000 chemiluminator (Thermo Fisher Scientific, Waltham,

592 MA, USA) with an enhanced chemiluminescent substrate for detection of horseradish

593 peroxidase (HRP; Merck, Darmstadt, Germany).

594

595 **Estimation of T_m values using fluorescence based thermal shift assay.** To estimate

596 the T_m values, we performed a fluorescence based thermal shift assay using ProteoStat

597 Thermal Shift Stability assay (ENZO Life Sciences, Farmingdale, NY, USA). 1 μg of

598 KRAS G12D was mixed with DMSO (2.5 %), RAS-SOS inhibitor (4 μM) or TUS-007

599 (4 μM) in 1x assay buffer containing a fluorescent indicator of protein destabilization,

600 ProteoStat TS Detection Reagent, and incubated under heating from 25 °C to 99 °C in

601 StepOne Plus Real-time PCR system (Thermo Fisher Scientific). The kinetics of

602 fluorescent signals were analyzed to calculate T_m values in Protein Thermal Shift

603 Software 1.3 (Thermo Fisher Scientific).

604

605 **Evaluation of KRAS degradation induced by TUS-007 in a cell-free system.** KRAS

606 G12D (final concentration: 5 ng/μL) and 26S proteasome (final concentration: 8 nM)

607 were incubated with TUS-007 (2, 3, 5, 10, 20, 40 μM), RAS-SOS inhibitor (40 μM),

608 RAS-SOS-NH_2 (40 μM) or DMSO in 20 mM Tris-HCl buffer (pH 7.5) containing 20%

609 glycerol for 3 h at 37 °C. To assess the effect of MLN on chemical knockdown, KRAS

610 G12D and 26S proteasome were incubated with DMSO or TUS-007 40 μM in the

611 presence or absence of MLN (1 μM) in the same condition. KRAS G12V (final

612 concentration: 5 ng/μL) and 26S proteasome (final concentration: 8 nM) were incubated

613 with TUS-007 at the indicated concentration or DMSO in 75 mM phosphate buffer,

614 containing 1% LABRASOL (Gattefossé, Saint-Priest, France), for 1 h at 37 °C. After

615 centrifugation at 14,000 ×*g* for 10 min, the supernatants were analyzed by SDS-PAGE,

616 followed by immunoblotting using an anti-KRAS antibody (1:1000, WH0003845MI for

617 G12D, Sigma-Aldrich; and 1:2000, F234 for G12V, Santa Cruz Biotechnology, Inc.,

618 Dallas, TX, USA). The immunoreactive bands were detected, as described above. The

619 DC_{50} values were calculated by a Rodbard approximation using the band intensity

620 obtained from four and three independent experiments for G12D. Immunoblotting was

621 performed as mentioned above.

622

623 **Evaluation of target degradation in HeLa cells by flow cytometry.** The expression

624 plasmid pMIR-DsRed-IRES-ecDHFR-HA-GFP was a kind gift from Dr. L. Hedstrom

625 (Brandeis University). Plasmid expressing human KRAS G12D was constructed by RF

626 cloning with some minor modifications. A full-length cDNA clone of human KRAS

627 (AK292510) was obtained from the National Institute of Technology and Evaluation

628 (Tokyo, Japan). Hybrid RF cloning primers were designed using RF-Cloning.org. All

629 PCR amplifications were performed with KOD-Plus-Neo (Toyobo Co. Ltd., Japan). The

630 plasmid DNA sequences encoding target proteins were determined using an ABI 3500

631 (Applied Biosystems, MA, USA). HA-GFP-fusion target protein- and DsRed-

632 expressing HeLa cells were treated with 1% DMSO or CANDDY molecules in serum-

633 free medium for 24 h. The cells were harvested using trypsin and resuspended in

634 fluorescence activated cell sorter (FACS) buffer. The cells were then analysed on a BD

635 FACSCanto II. Data were analysed using FlowJo software (FlowJo LLC).

636

637 **Cell proliferation assay.** To examine the effect of TUS-007 on cell proliferation, the

638 WST-8 assay (Cell Count Reagent SF; Nacalai Tesque, Kyoto, Japan) was performed.

639 RAS-less MEF cells, expressing human RAS, were plated in 96-well plates at a density

640 of 3×10^3 cells per well, cultured overnight, then treated with the indicated

641 concentrations of TUS-007 in 4% FBS containing medium (KRAS G12D), 10% FBS

642 containing medium (KRAS G12V) or serum-free medium (KRAS G12C, wt KRAS,

643 HRAS, NRAS) for 72 h. After incubation, cell viability was measured

644 spectrophotometrically using the WST-8 reagent. The culture medium was removed and

645 WST-8 reagent was mixed with the growth medium at a ratio of 1:10 (with a final

646 volume of 110 μL) and added to each well. The cells were incubated in an atmosphere

647 of 5% CO_2 at 37 °C for 1 to 2 h, and the absorbance at 450 nm was measured using the

648 aforementioned Synergy HT multi-channel microplate reader (BioTek Instruments,

649 Inc.).

650

651 **Evaluation of TUS-007 specificity in cells.** RAS-less MEFs were used to evaluate the

652 selective degradation by TUS-007. RAS-less MEFs expressing one of the human WT

653 RAS members (KRAS WT, HRAS WT, or NRAS WT) or KRAS G12C were plated

654 into 6-well plates at a density of 3×10^4 cells per well, cultured overnight, and treated

655 with the indicated concentrations of TUS-007 in serum-free medium for 72 h. RAS-less

656 MEFs expressing KRAS G12D or G12V were plated into 96-well plates at a density of

657 3×10^3 cells per well, cultured overnight, and treated with the indicated concentrations

658 of TUS-007 in 4% FBS or 10% FBS containing medium, respectively, for 72 h. The

659 cells were lysed using RIPA buffer (Nacalai Tesque., Kyoto, Japan). The lysates were

660 centrifuged at 18,000 ×*g* for 10 min. The supernatants were analyzed by western

661 blotting using mouse monoclonal antibodies specific to KRAS (1:1000,

662 WH0003845MI; Sigma-Aldrich) and glyceraldehyde 3-phosphate dehydrogenase

663 (GAPDH, 1:10000, sc-32233; Santa Cruz Biotechnology, Inc.) and rabbit polyclonal

664 antibodies specific for HRAS (1:1000, 18295-1-AP; Proteintech, Rosemont, IL, USA)

665 and NRAS (1:1000, 10724-1-AP, Proteintech). Immunoreactive bands were detected

666 using iBright CL1000 chemiluminator or LAS 3000 (Fujifilm, Tokyo, Japan) with an

667 enhanced chemiluminescent substrate for the detection of horseradish peroxidase (HRP;

668 Merck, Darmstadt, Germany). The intensity of the RAS band was quantified using

669 ImageJ software and normalized to the intensity of the GAPDH band.

670

671 **Measurement of KRAS protein levels in cells by western blotting.** SW620-Luc and

672 SW1990 cells were treated with 1% DMSO or TUS-007 in serum-free medium for 12

673 or 48 h (SW620-Luc cells) and 12 or 72 h (SW1990 cells). The cells were lysed using a

674 RIPA buffer (Nacalai Tesque., Kyoto, Japan). The precipitates were separated from the

675 soluble fraction by centrifugation at 18,000 ×*g* for 20 min. The supernatants were

676 analyzed by western blotting with mouse monoclonal antibodies specific for KRAS

677 (1:1000, WH0003845MI; Sigma-Aldrich) and GAPDH (1:20000, sc-32233; Santa Cruz

678 Biotechnology, Inc.). The immunoreactive bands were detected by LAS-3000, as

679 described above. The intensity of the KRAS band was quantified using ImageJ software

680 and normalized to the intensity of the GAPDH band.

681

682 **Evaluation of caspase activity.** To measure caspase activity, SW1990 cells were plated

683 onto 96-well white plates and 96-well clear plates, at a concentration of 8×10^3

684 cells/well, in a medium containing 10% FBS. The plates were incubated overnight

685 without CO_2 equilibration at 37 °C. The medium was replaced with medium containing

686 2% FBS, DMSO, 100 μM TUS-007, 3 μM MLN2238, or 2.5 μM NAEi and incubated

687 for 96 h. SW620-Luc cells were plated onto 96-well white plates and 96-well clear

688 plates at 2×10^3 cells/well in medium containing 10% FBS. After overnight incubation,

689 the medium was replaced with FBS-free medium containing 1% L-glutamine, DMSO,

690 and 25, 100, or 500 μM TUS-007 for 48 h. The caspase 3/7 Glo assay (Promega,

691 Madison, WI, USA) was performed on the white plates according to the manufacturer's

692 protocol. The chemiluminescence intensity was measured with a Synergy HT plate

693 reader (BioTek). The cell viability was measured in the clear plates using the WST-8

694 assay, as described above. Caspase 3/7 activity was obtained as the chemical

695 luminescence intensity of the caspase 3/7 Glo assay normalized to the cell viability.

696

697 **Analysis of apoptosis by flow cytometry.** SW1990, SW620-Luc, and HT-29 cells

698 were seeded in 24-well plates, followed by the addition of compounds at the indicated

699 concentrations. After incubation for 12 or 48 h (SW620-Luc, HT-29) and 12 or 72 h

700 (SW1990), the cells were harvested using trypsin, washed with phosphate-buffered

701 saline (PBS), and pelleted by centrifugation at 110 ×*g* for 5 min. The cells were

702 resuspended in 85 μL of binding buffer (Annexin V-FITC Kit, Medical & Biological

703 Laboratories Co., Ltd., Nagoya, Japan). Subsequently, 10 μL of annexin V-FITC and 5

704 μL of propidium iodide (PI) were added to each sample, followed by incubation in the

705 dark at room temperature for 15 min. After incubation, 400 μL of binding buffer was

706 added to each sample on ice. The cells were then analyzed using a FACSCanto II

707 fluorescence-activated cell sorter (BD Biosciences, Santa Clara, CA, USA) to detect the

708 fluorescein isothiocyanate (FITC) signal with excitation and emission filter wavelengths

709 of 488 nm and 580 nm, respectively, to detect the PI signal. Data were analyzed using

710 FlowJo software (FlowJo, Eugene, OR, USA).

711

712 **Subcutaneous xenograft model.** SW620-Luc (3×10^7 cells/mL) and SW1990 (5×10^7

713 cells/mL) cells were suspended in PBS, and 100 μL of the single-cell suspension was

714 transplanted subcutaneously into the right flanks of BALB/cA-nu/nu mice using a 26 G

715 syringe. Tumor volumes were calculated as the tumor length × width^2 × 0.5. When the

716 tumor volumes reached approximately 100 mm^3, the mice were randomized into

717 treatment and control groups of 6 to 8 animals per group. For i.p. treatment, TUS-007

718 was dissolved in DMSO and then diluted to a final concentration of 10% DMSO in 20%

719 polyethylene glycol (PEG) 400/Tween 80 (1:1 ratio). The TUS-007 solution was

720 administered intraperitoneally into the tumor-bearing mice at a dose of 80 mg/kg every

721 three days. The control mice were treated with the PEG/Tween vehicle alone. For p.o.

722 treatment, TUS-007 was suspended in 0.5% (w/v) carboxymethyl cellulose (CMC) and

723 administered p.o. at a dose of 80 mg/kg every three days. CMC (0.5% w/v) was

724 administered to control mice. Cetuximab was administered to an additional group of

725 SW620-Luc-implanted mice at a dose of 1 mg/mouse every three days.

726

727 **Orthotopic xenograft model.** The pGL4.51 (Luc2/CMV/Neo) vector (Promega) was

728 transfected into SW1990 cells. Successfully transfected cells were selected using G418.

729 SW1990-Luc cells were mixed with growth factor-reduced Matrigel (BD Biosciences)

730 on ice, at a ratio of 1:1 (v/v), to obtain a final cell density of 1.5×10^4 cells/μL. Ten

731 microliters of the cell suspension was injected directly into the pancreas of BALB/cA-

732 nu/nu mice using a 27 G syringe. Three days after cell transplantation, TUS-007

733 treatment was initiated in six mice. TUS-007 was suspended in 0.5% (w/v) CMC and

734 administered orally at a dose of 160 mg/kg every 3 days. CMC (0.5% w/v) was

735 administered to control mice (n = 6). Tumor luciferase activity was monitored based on

736 the bioluminescence intensity. Fifty microliters of D-luciferin (30 mg/mL in saline) was

737 injected subcutaneously in mice (Promega). Twenty minutes after the injection,

738 bioluminescence images were obtained using an IVIS Lumina LT (Perkin Elmer,

739 Waltham, MA, USA) with an exposure time of 15 s while the mice were under

740 isoflurane anesthesia (Wako, Tokyo, Japan).

741

742 **Measurement of RAS levels and downstream signaling molecule activation in**

743 **xenograft tumors.** KRAS expression in xenograft tumors and wt RAS protein

744 expression in pancreas were evaluated by immunohistochemistry and western blot

745 analysis. Tumor tissue and pancreas were harvested from the mice harboring

746 subcutaneous xenografts on day 21 of the TUS-007 administration. Tumor tissues were

747 harvested from the orthotopic xenograft mice on day 24 after the TUS-007

748 administration for consecutive 3 days starting on day 21. A portion of each sample was

749 fixed in 4% paraformaldehyde (Nacalai Tesque., Kyoto, Japan), embedded in paraffin,

750 then cut into 5 μm-thick sections. The sections were deparaffinized and incubated in

751 0.3% hydrogen peroxide in methanol for 30 min, and antigen retrieval was performed

752 using a 10 mM citrate buffer (pH 6.0) at 121 °C for 20 min. Tumor tissues were

753 subsequently blocked with 1% bovine serum albumin (BSA) in PBS for 30 min and

754 stained with primary antibodies specific for human KRAS (1:200, 12063-1-AP;

755 Proteintech), diluted in 1% BSA, followed by HRP-labeled secondary antibodies

756 (1:600, ab6721; Abcam, Cambridge, UK) in 1% BSA for 30 min at room temperature.

757 The sections were counterstained with hematoxylin and visualized with

758 diaminobenzidine (1.02924.0001; Merck). Digital images were obtained at 40×

759 magnification using a model BZ-9000 microscope (Keyence, Osaka, Japan). The area of

760 KRAS staining was quantified using ImageJ software, and the perimeter-to-area ratio

761 (KRAS-positive area/section) was calculated for a total of 30 images of 6 tumor

762 sections from each group. The remaining part of each tumor sample was homogenized

763 in a cell-lysis buffer (50 mM triethanolamine, 50 mM KCl, 5 mM $MgCl_2$, 0.25 M

764 sucrose, 1 mM phenylmethylsulfonyl fluoride, proteinase inhibitors (Nacalai Tesque.,

765 Kyoto, Japan), 1 mM dithiothreitol, and ribonuclease inhibitor (0.2 unit/μl, TaKaRa

766 Bio., Shiga, Japan) for western blot analysis, as described above. Mouse monoclonal

767 antibodies specific for KRAS (1:1000, WH0003845MI; Sigma-Aldrich), HRAS

768 (1:1000, 18295-1-AP; Proteintech, Rosemont, IL, USA), NRAS (1:1000, 10724-1-AP,

769 Proteintech) and GAPDH (1:20000, sc-32233; Santa Cruz Biotechnology, Inc.) and

770 rabbit antibodies specific for p-Erk1/2 (phospho-p44/42 MAPK) (1:1000, #4370; Cell

771 Signaling Technology, Beverly, MA, USA), Erk1/2 (p44/42 MAPK) (1:1000, #4695;

772 Cell Signaling Technology), p-Akt (1:2000, #4060; Cell Signaling Technology), and

773 Akt (1:2000; #4691; Cell Signaling Technology) were used for the

774 immunohistochemical staining. The immunoreactive bands were detected by LAS-3000

775 as described above. Quantitative analysis of the western blots was performed using

776 ImageJ software, and the results were normalized to the GAPDH band intensity.

777

778 **Measurement of apoptosis in xenograft tumors.** DNA fragmentation in the tumor

779 tissues was evaluated by a TdT-mediated dUTP nick-end labeling (TUNEL) assay.

780 Paraffin-embedded tissue sections (5 μm thick) were deparaffinized. The TUNEL

781 reaction was performed using the DeadEnd Fluorometric TUNEL System (Promega),

782 according to the manufacturer's instructions. Fluorescence images were acquired using a

783 BZ-9000 fluorescence microscope (Keyence). TUNEL-positive cells were identified

784 and counted using ImageJ software. In total, 30 images of 6 tumor sections were

785 analyzed from each group.

786

787 **Determination of TUS-007 in pancreas.** BALB/cA mice were treated i.p. with TUS-
788 007, and pancreas tissue was collected at suitable time points. Approximately 30-60 mg
789 of tissue was homogenized in 0.6 mL of tissue-lysis buffer (50 mM Tris-HCl pH 8.0, 20
790 mM EDTA, 10 mM NaCl, 1% SDS) by Micro Smash MS-100 using stainless (5.5 ϕ) and
791 zirconia (1.0 ϕ) beads (TOMY SEIKO CO., LTD., Tokyo, Japan), and 1 μL propyl p-
792 hydroxybenzoate (4 mg/mL in DMSO) was added to each sample as an internal standard.
793 Lysates were centrifuged at 18,000 ×*g* for 10 min and 2.25 mL of methanol/chloroform
794 (ratio of 2:1) was added to the supernatants and the mixture was allowed to stand for 30
795 min at room temperature. Chloroform and distilled water (0.75 mL each) were added and
796 samples were centrifuged at 1,500 ×*g* for 15 min. The layer of chloroform was collected.
797 The supernatants were dried under reduced pressure and redissolved in the mobile phase.
798 TUS-007 was determined by HPLC (Alliance e2695, Waters Corporation., MA, USA)
799 using COSMOSIL® C18-AR-II column (150×4.6 mm, Nacalai Tesque., Kyoto, Japan) in
800 the isocratic elution mode with 0.1% trifluoroacetic acid (TFA) in 50:50 (v/v)
801 acetonitrile/water mobile phase at a flow rate of 1.0 mL/min. All reagents for the assay
802 were purchased from Nacalai Tesque. (Kyoto, Japan).

803

804 **Degradation of MDM2 in HCT-116 cells.** HCT-116 human colon-cancer cells were

805 treated with 1% DMSO or TUS-007 in serum-free medium for 24 h. The cells were

806 lysed using a RIPA buffer (Nacalai Tesque). The precipitates were separated from the

807 soluble fraction by centrifugation at 18,000 ×*g* for 20 min. The supernatants were

808 analyzed by western blotting using a rabbit polyclonal antibody specific for MDM2

809 (1:1000, sc-965, Santa Cruz Biotechnology, Inc.) and GAPDH (1:20000, sc-32233;

810 Santa Cruz Biotechnology, Inc.). The immunoreactive bands were detected by LAS-

811 3000, as described above. The intensity of the MDM2 band was quantified using

812 ImageJ software and normalized to the intensity of the GAPDH band.

813

814 **Statistical analyses.** Statistical significance was determined with JMP® Pro 14 (SAS

815 Institute Inc., Cary, NC, USA). An unpaired *t*-test was used to compare pairs of groups

816 under the assumption of normality. A one-way ANOVA with Dunnett's post hoc

817 analysis was used to compare sets of three or more groups. P-values < 0.05 were

818 considered statistically significant.

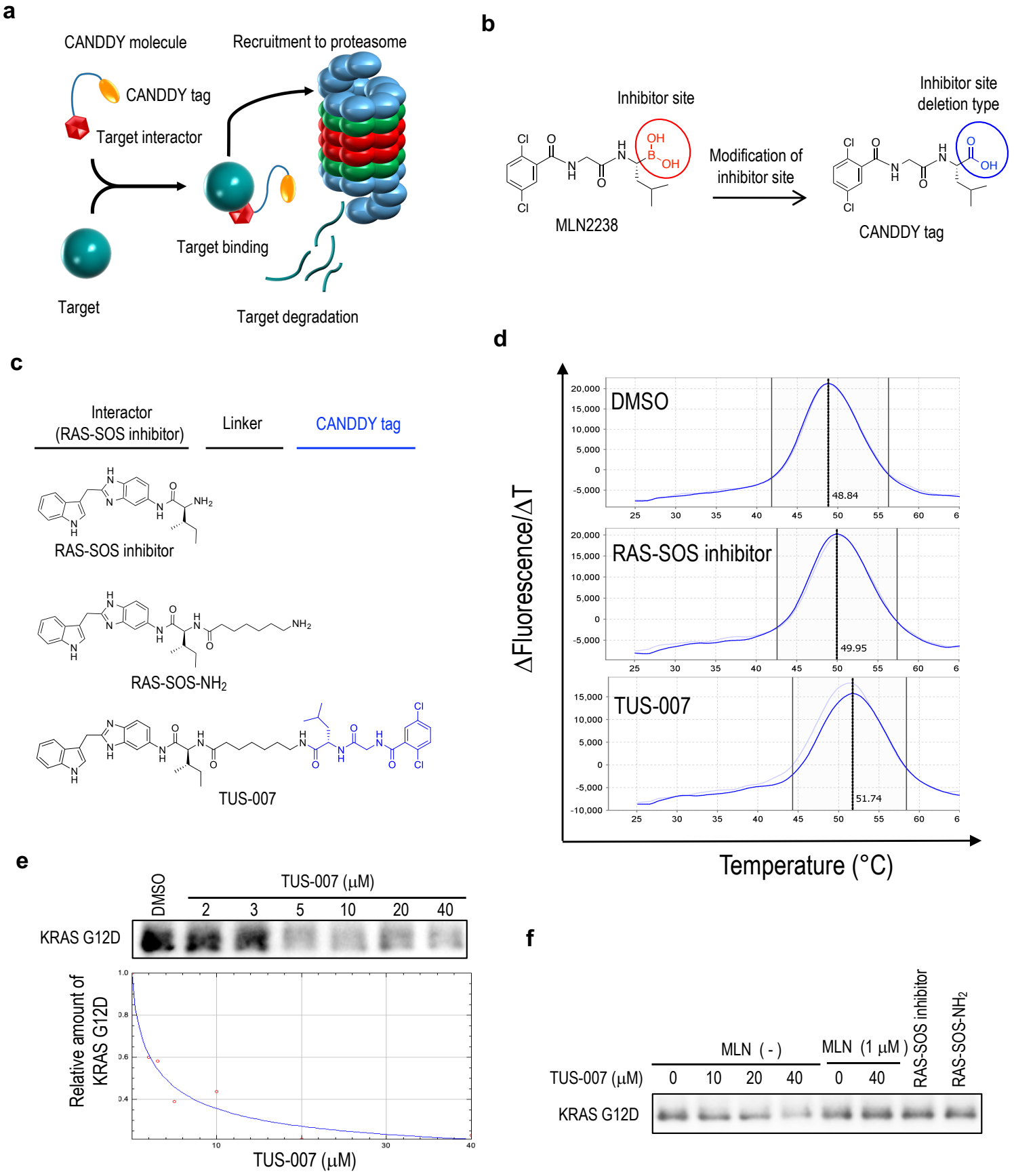

Fig. 1. RAS chemical knockdown in cell free assays.
a, Principle of the CANDDY technology. Each CANDDY molecule includes a target interactor (burgundy hexagon) and a CANDDY tag (yellow oval). The target protein is bound by the CANDDY molecule *via* the target interactor and is directly degraded by proteasome via the CANDDY tag. **b,** The CANDDY tag was synthesized by chemically inactivating the inhibitor site of MLM2238 (MLN). **c,** Structures of the RAS-SOS inhibitor (ref. 5), RAS-SOS-NH_2, and TUS-007. **d,** KRAS G12D was mixed with DMSO, RAS-SOS inhibitor (4 μM) or TUS-007 (4 μM) and incubated under heating from 25 °C to 99 °C. The denature of KRAS G12D was monitored by the fluorescence. The typical curve of each group was shown. **e,** The correlation between relative amount of KRAS G12D and concentration of TUS-007 were approximated with Rodbard using the means of 3 independent examinations. The DC50 was estimated about 4 μM. **f,** TUS-007 induced KRAS G12D chemical knockdown by 26S proteasome in a cell free assay. KRAS G12D was incubated with 26S proteasome and agents as indicated for 3 h.

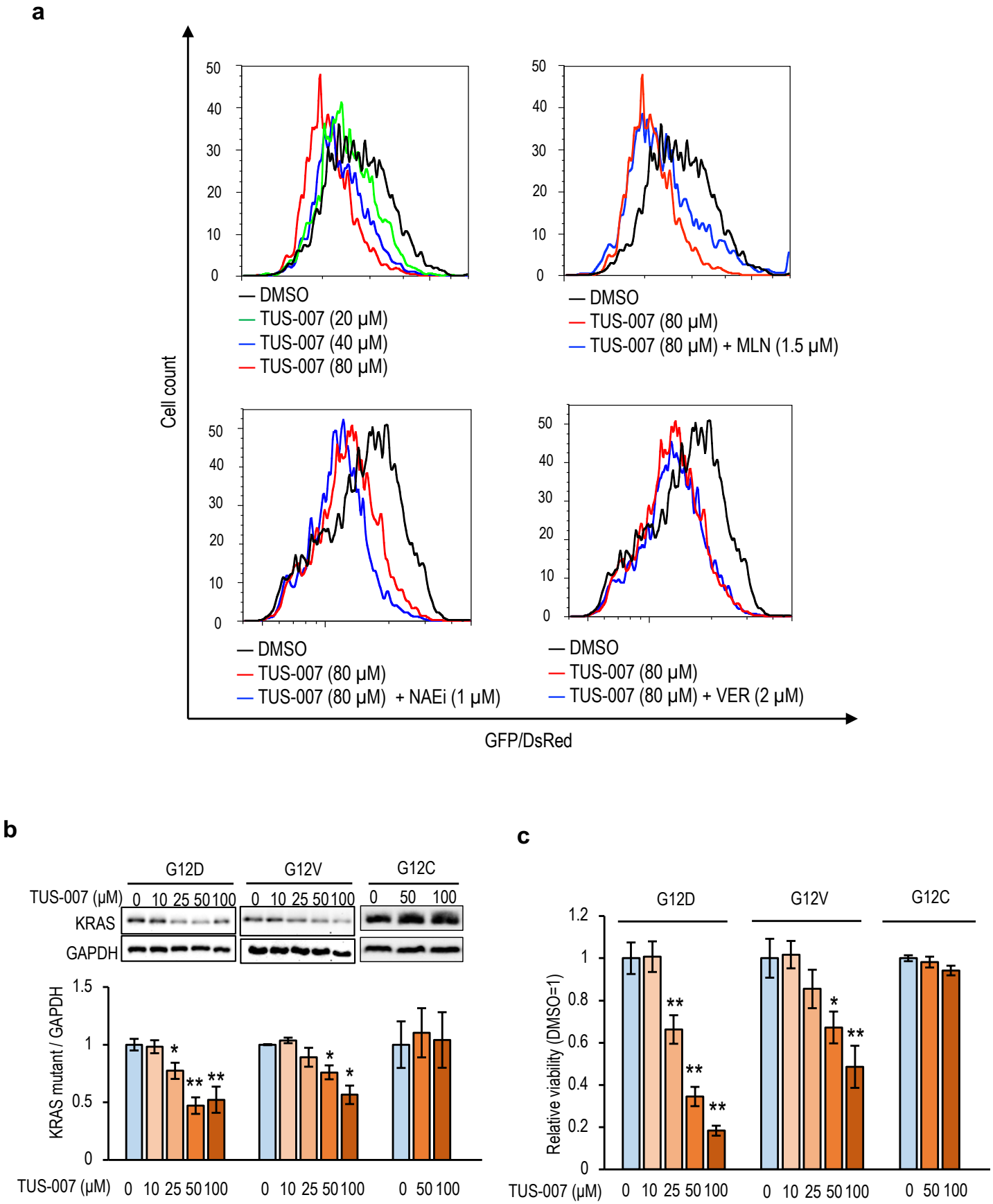

Fig. 2. RAS chemical knockdown in cells.
a, TUS-007 induced chemical knockdown was independent of ubiquitination**.** GFP fused KRAS G12D and DsRed were transiently expressed in HeLa cells. The cells were treated with TUS-007 in the presence of a proteasome inhibitor (MLN), a ubiquitination inhibitor (NAEi) and a molecular chaperon inhibitor (HSP70 inhibitor: VER-155008) for 24 h. **b & c,** RAS-less MEFs expressing KRAS G12D, G12V or G12C were incubated with TUS-007 for 72 h. Representative blots of KRAS are shown (**b**). The relative amounts of KRAS mutants normalized to GAPDH are shown in the bar graph (mean ± SEM; n = 3–4). The cell viability was also measured (mean ± SEM; n = 3–4) (**g**). *P < 0.05 and ** P < 0.01 vs. DMSO. TUS-007 induced chemical knockdown did not cause non-specific cytotoxicity.

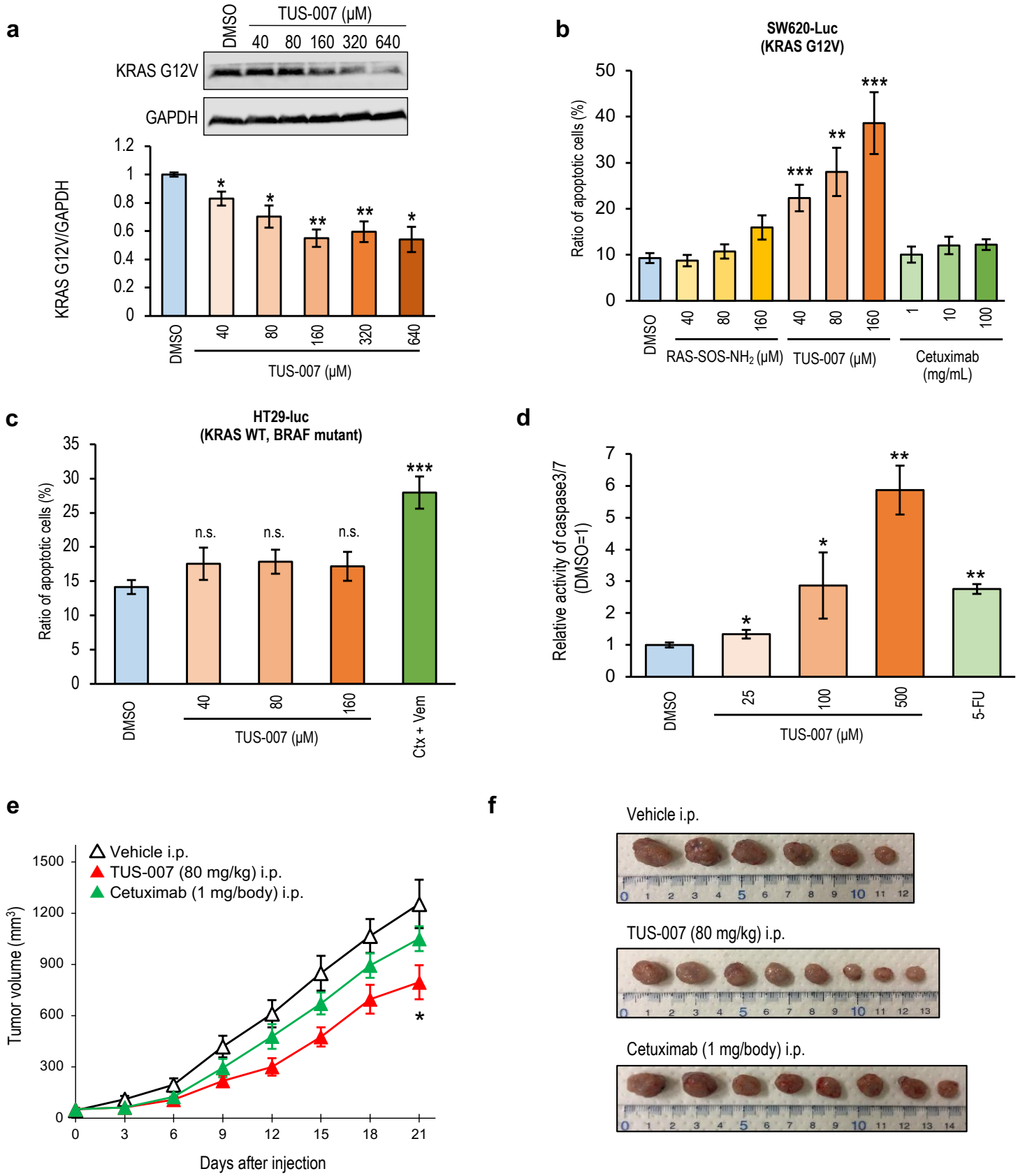

Fig. 3. Chemical knockdown and tumor suppression *in vitro* and *in vivo* in KRAS G12V-driven human colon cancer cells by TUS-007 treatment.

a, Immunoblotting analysis of KRAS G12V chemical knockdown in SW620-Luc cells treated with TUS-007 for 48 h at the indicated doses. The KRAS band intensity was normalized to that of GAPDH (mean ± SEM; n = 3). *P < 0.05 and **P < 0.01 vs. DMSO. **b & c,** The ratio of apoptotic cells were analyzed in colon cancer SW620-Luc cells (**b**) and HT29-Luc cells (**c**), a KRAS-independent, BRAF-dependent cell line (Ctx + Vem: 100 μg/ml cetuximab and 40 μM vemurafenib). Cells were treated with each compound for 48 h in terms of the number of annexin V-positive/PI-negative apoptotic cells detected by flow cytometry (mean ± SEM; n = 2–5). **P < 0.01, and ***P < 0.001 vs. DMSO. **d,** Relative activity of caspase 3/7 in SW620-Luc cells treated with TUS-007 or 5-fluorouracil (5-FU) for 48 h (mean ± SEM; n = 3). *P < 0.05 and **P < 0.01 vs. DMSO. **e,** Tumor volume in mice with SW620-Luc cells transplanted subcutaneously and treated with i.p. administration every 3 days (mean ± SEM; n = 6–8). *P < 0.05 vs. vehicle alone. **f,** Tumors of SW620-Luc cells at day 21 from the same mice shown in **e** (n = 6–8).

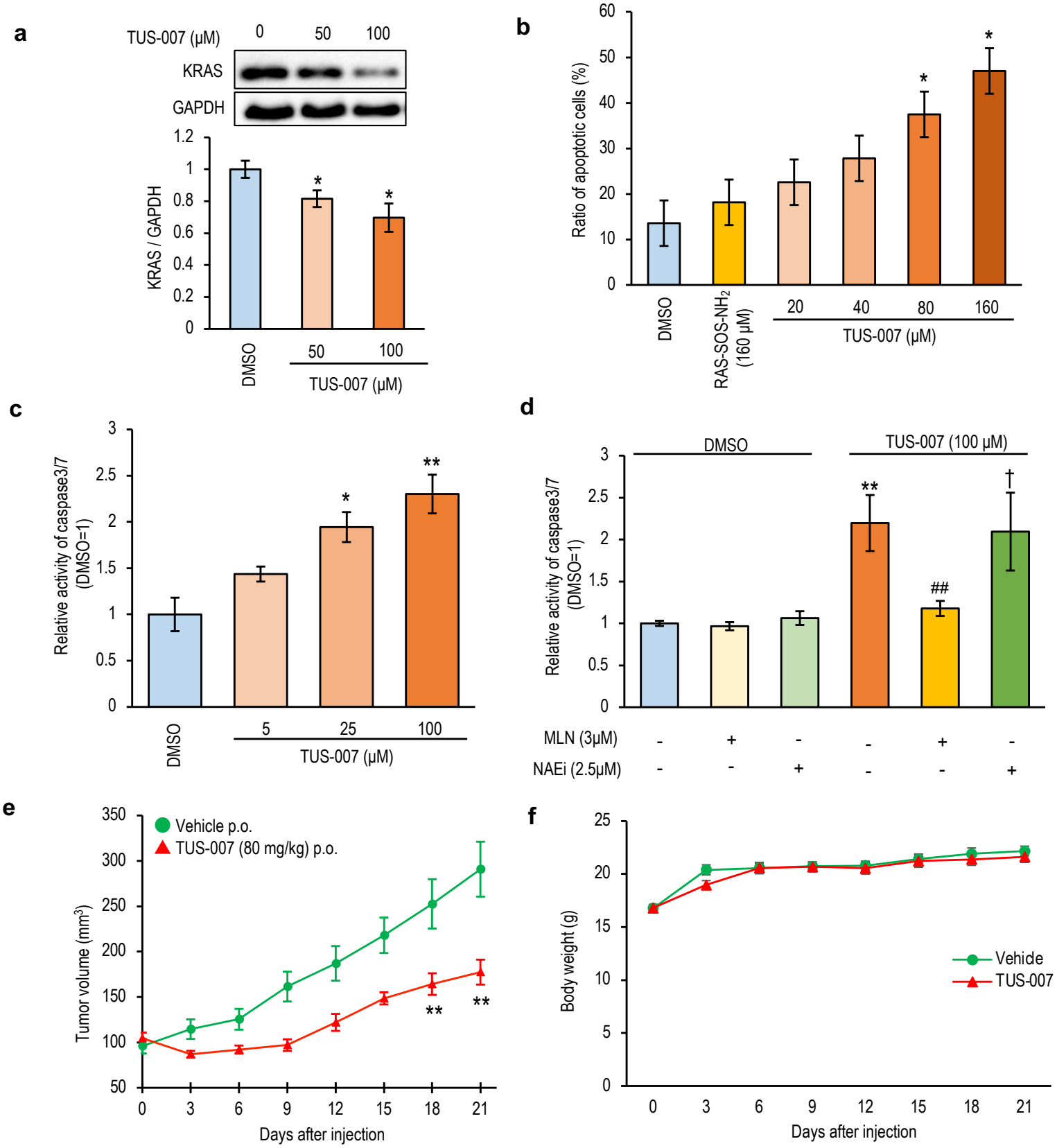

Fig. 4. Chemical-knockdown and tumor suppression *in vitro* and *in vivo* in KRAS G12D-driven human pancreatic cancer cells by TUS-007 treatment.

a, KRAS G12D chemical knockdown induced by TUS-007 in SW1990 cells. SW1990 cells were treated with TUS-007 for 72 h and analyzed by immunoblotting. The KRAS G12D band intensity was normalized to that of GAPDH (mean ± SEM; n = 4). *P < 0.05 vs. DMSO. **b,** The proportion of annexin V-positive apoptotic SW1990 cells treated with DMSO, RAS-SOS-NH_2 or TUS-007 for 72 h (mean ± SEM; n = 3). *P < 0.05 vs. DMSO or RAS-SOS-NH_2. **c,** TUS-007 increased the caspase 3/7 activity in SW1990 cells after treatment for 96 h (mean ± SEM; n = 3). *P < 0.05 and **P < 0.01 vs. DMSO. **d,** Caspase 3/7 activation by TUS-007 was proteasome dependent and ubiquitination independent. SW1990 cells were treated with the agents for 96 h (mean ± SEM; n = 3). **P < 0.01 vs. DMSO, ##P < 0.01 vs. TUS-007 (100 μM) only, and †no statistically significant difference compared with TUS-007 (100 μM) only. **e,** Tumor volume in mice with SW1990 cells transplanted subcutaneously and treated with p.o. administered TUS-007 or vehicle (mean ± SEM; n = 6–9). The agents were administered every 3 days. **P < 0.01 vs. vehicle alone. **f,** Body weight changes in mice with SW1990 cells transplanted subcutaneously (mean ± SEM; n = 6–9).

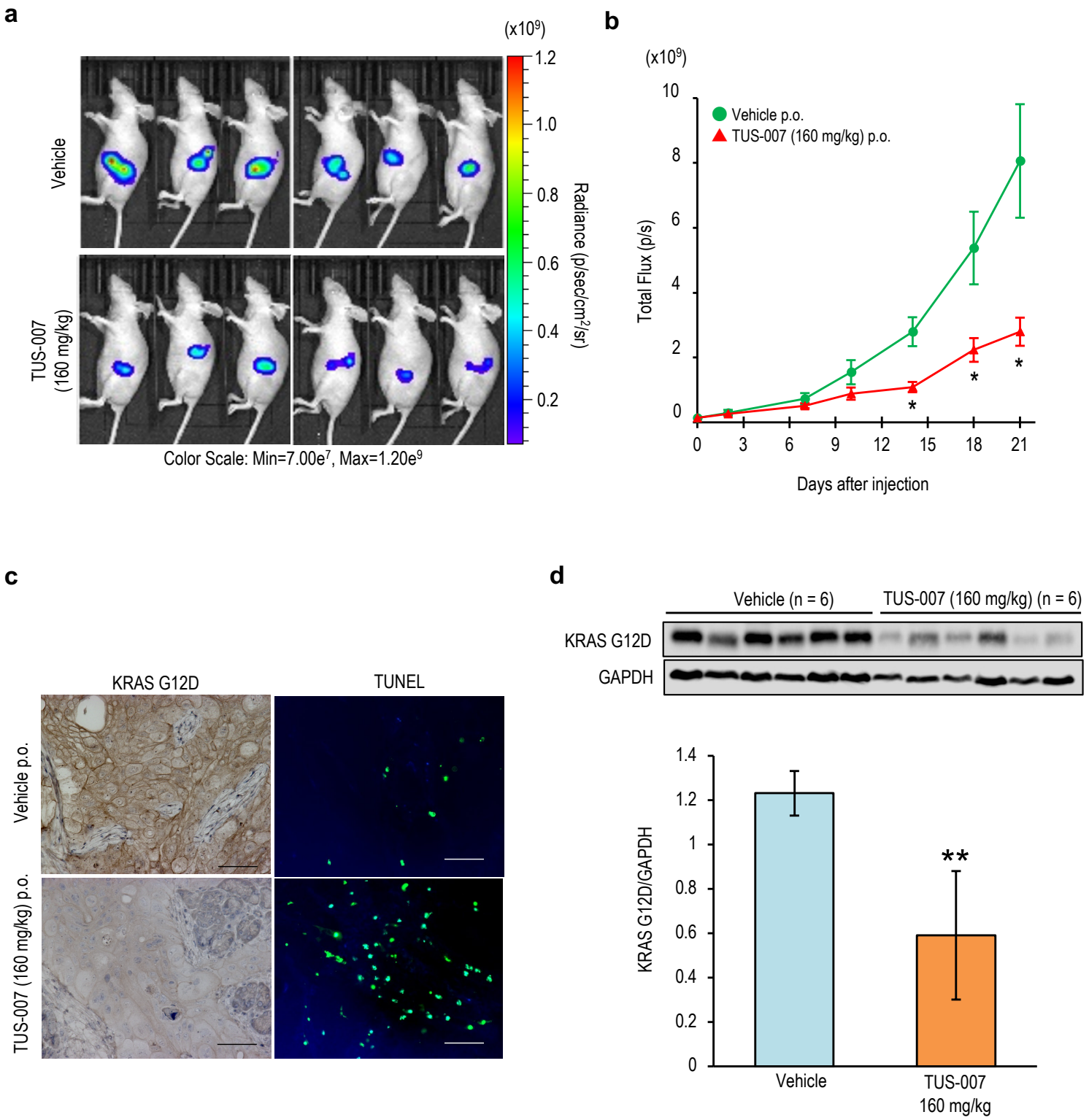

Fig. 5. TUS-007 suppresses the growth of KRAS G12D-positive orthotopic pancreatic tumors.
a, Images showing the luciferase activity and total flux in orthotopic tumors transplanted SW1990-Luc cells *in vivo*. **b,** Tumor growth (bioluminescence) in identical mice treated with vehicle or TUS-007 administered p.o. every 3 days. (mean ± SEM; n = 6). *P < 0.05 vs. vehicle alone. **c,** Representative histochemical staining of KRAS and TUNEL in orthotopic tumor sections from the same mice used in **a**. The scale bar is 60 μm. **d,** Immunoblotting of KRAS G12D in tumor lysates from the same mice used in **a**. The bar graph shows quantification of KRAS G12D normalized to GAPDH (mean ± SEM; n = 6). **P < 0.01 vs. vehicle alone.

1 **Supplementary Information for "*In vivo* KRAS G12D/V Degradation Mediated by**

2 **CANDDY Using a Modified Proteasome Inhibitor"**

3 Satoshi Imanishi, Lijuan Huang, Shoko Itakura, Masamichi Ishizaka, Yoichi Iwasaki,

4 Tomohiro Yamaguchi, and Etsuko Miyamoto-Sato.

5

Text S1. Synthesis of CANDDY molecules

General. Nuclear magnetic resonance (NMR) spectra were recorded on a Bruker BioSpin AVANCE600 spectrometer operating at 600 MHz for ^{1}H-NMR. Chemical shifts were reported in the scale relative to CD_3OD as an internal reference. Fast-atom bombardment mass spectrometry was performed on a JEOL JMS-700. Column chromatography was performed with silica gel 60 (75 mm) purchased from Nacalai Tesque, Inc. PLC silica gel 60 was purchased from Merck KGaA. Reversed phase liquid chromatography was performed with high performance liquid chromatography (HPLC) (Shimadzu Co., Ltd), with a YMC-Pack ODS-A or Inertsil ODS-4 (GL Science) (250 × 4.6 mm), an LC-6AD pump, and a RID-10A detector (Shimadzu Co., Ltd). HPLC experiment was performed with isocratic condition A (MeCN/H_2O/TFA, 70:30:0.1; flow rate, 1 mL/min) for compounds **1–3**, and condition B (MeCN/H_2O/TFA, 55:45:0.1; flow rate, 1 mL/min) for TUS-007.

H-Gly-OtBu · HCl and 2,5-dichlorobenzoic acid were purchased from Ark Pharm. H-Leu-OtBu · HCl and H-Phe-OtBu · HCl were purchased from Watanabe Chemical Industry.

22 Synthesis of TMP-NH_2 was based on a previous report[26]. The synthesis of RAS-SOS

23 inhibitor (**4**) and RAS-SOS-NH_2 (**5**) was based on a previous report[15]. A part of the

24 compound was synthesized by NARD Institute. Ltd. (Kobe, Japan).

25

26 **The synthesis of TUS-007.**

27 TUS-007 was synthesized as shown below. Some of the compounds were synthesized

28 by the NARD Institute. Ltd. (Kobe, Japan).

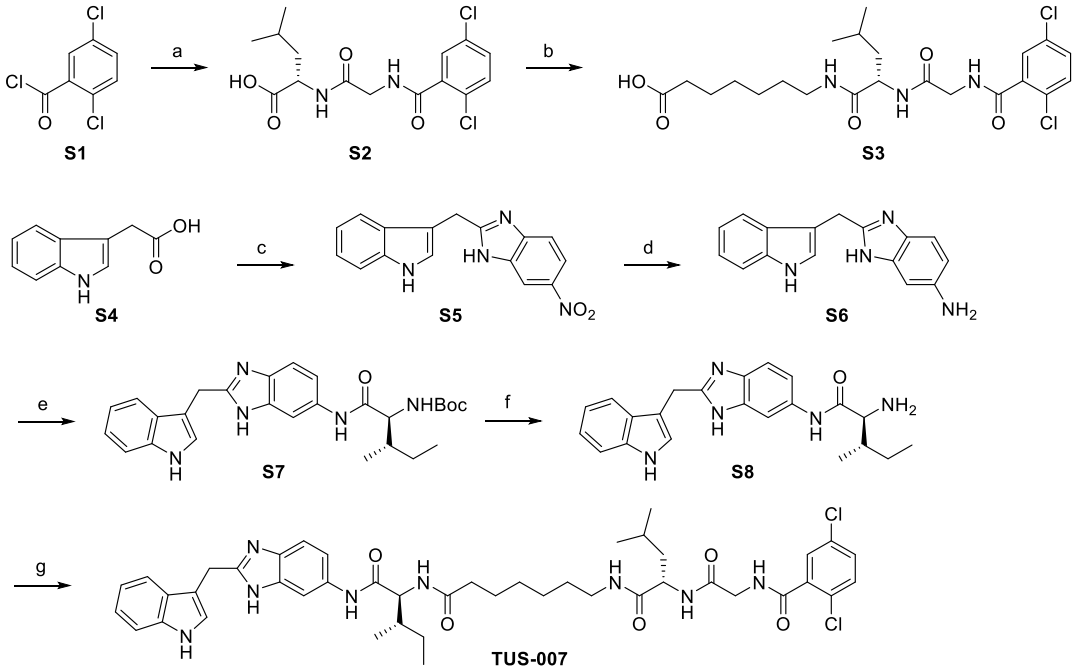

Reagent and conditions: (a) Glycyl-L-luecine, 1N NaOHaq.,THF 0°C, 88%; (b) (i) HOSu, EDC-HCl, CH_2Cl_2, 0°C to rt, (ii) 7-Amino-heptanoic acid, Triethylamine, DMF, 0°C to rt, 72%; (c) (i) CDI, THF, 0°C to rt; 4-Nitro-1,2-phenylenediamine, 47°C, (ii) AcOH, reflux, 88%; (d) H_2, Pd/C, MeOH, rt, 62%; (e) *N*-Boc-L-Isoleucine, COMU, DIPEA, MeCN, 0°C to rt, *quant.*; (f) TFA, CH_2Cl_2, rt, 76%; (g) **S3**, HATU, DIPEA, DMF, 0°C to rt, 53%.

29

30 To a solution of glycyl-L-leucine (125 g, 664 mmol) in 1N NaOH*aq*. (1.3 L)

31 with tetrahydrofuran (THF: 550 mL), 2,5-dichlorobenzoyl chloride (127 g, 604 mmol)

32 in THF (250 mL) was added dropwise at 0°C. After stirring for 2 h at the same

33 temperature, the resulting solution was acidified (ca. pH2) with 2N HCl*aq*. and

34 extracted with $CHCl_3$ (total 3 L). The combined organic layer was washed with brine,

35 dried over $MgSO_4$, filtered, and concentrated *in vacuo*. The residue was suspended in

36 diisopropyl ether (IPE: 1.2 L) and stirred for 30 min at 50°C. The resulting suspension

37 was cooled to room temperature, and a precipitate was filtered, washed with IPE (500

38 mL), and thus **S2** (194 g, 88 % yield, white solid) was obtained.

39 (i) To a solution of **S2** (194g, 536 mmol) in CH_2Cl_2 (1.6 L), *N*-hydroxysuccinimide

40 (HOSu: 2.5 g, 804 mmol) and 1-ethyl-3-(3-dimethylaminopropyl) carbodiimide

41 hydrochloride (EDC-HCl: 54 g, 804 mmol) were added at 0°C under Ar atmosphere.

42 After stirring for 3 h at room temperature, the resulting solution was washed with water

43 (1 L) three times, dried over $MgSO_4$, filtered, and concentrated *in vacuo*. (ii) The

44 residue (309 g) was dissolved in DMF (1.5 L) at Ar atmosphere, and 7-aminoheptanoic

45 acid (77.8 g, 536 mmol) and triethylamine (178 mL) were added to the solution at 0°C.

46 After stirring overnight at room temperature, 1N HCl*aq*. (1.5 L), water (1 L) and AcOEt

47 (3 L) were added and extraction was performed using AcOEt (1.5 L). The combined

48 organic layer was dried over Na_2SO_4, filtered, concentrated *in vacuo* and azeotroped

49 with toluene. The residue (394 g) was purified by silica gel column chromatography

50 (4.5 kg, elution with 0-5 % MeOH/$CHCl_3$) and thus **S3** (190 g, 72 % yield, white solid)

51 was obtained. **S3**: ^{1}H-NMR (400 MHz, DMSO-d_6) δ 0.84 (3H, d, J = 6.4 Hz), 0.87 (3H,

52 d, J = 6.4 Hz), 1.18-1.27 (4H, m), 1.35-1.60 (7H, m), 2.16 (2H, t, J = 7.3 Hz), 2.94-3.09

53 (2H, m), 3.82-3.92 (2H, m), 4.26-4.31 (1H, m), 7.53 (3H, s), 7.92 (1H, t, J = 5.5 Hz),

54 7.96 (1H, d, J = 8.2 Hz), 8.78 (1H, t, J = 6.0 Hz), 11.96 (1H, s).

55 (i) To a solution of indol-3-ylacetic acid (100 g, 571 mmol) in THF (200 mL),

56 1,1'-Carbonyldiimidazole (CDI: 109 g, 674 mmol) was added in portions over 15 min at

57 0°C under Ar atmosphere. After stirring for 30 min at room temperature,

58 4-nitro-1,2-phenylenediamine (96.2 g, 628 mmol) was added, and stirred for 30 min at

59 same temperature. The resulting solution was warmed to 47°C and concentrated *in*

60 *vacuo* after stirring overnight. (ii) The residue was dissolved in AcOH (2 L) with

61 ice-cooling and heated to reflux for 2 h. The resulting solution was concentrated *in*

62 *vacuo* and azeotroped with toluene. The residue was dissolved in AcOEt (1 L), and

63 insoluble portion was filtered on a Celite-pad, then washed with AcOEt (0.8 L). The

filtrate was washed with water (1.5 L) and brine (1 L), dried over Na_2SO_4, and concentrated *in vacuo*. The residue (298 g) was purified by silica gel column chromatography (2 kg, elution with 0-30 % AcOEt/$CHCl_3$) and thus **S5** (146 g, 88 % yield, brown amorphous) was obtained.

To a solution of **S5** (146 g, 500 mmol) in MeOH (1 L), Pd/C (20.0 g) was added and stirred overnight at room temperature under H_2 atmosphere. The resulting solution was filtered on a Celite-pad, washed with MeOH (2 L), and concentrated *in vacuo*. The residue was purified by silica gel column chromatography (3.0 kg, elution with 5-20 % MeOH/$CHCl_3$) and thus **S6** (85.4 g, 62 % yield, black solid) was obtained.

To a solution of **S6** (81.9 g, 351 mmol) in MeCN (1.2 L), *N*-ethyldiisopropylamine (DIPEA: 119 mL) and (1-Cyano-2-ethoxy-2-oxoethylidenaminooxy)dimethylamino-morpholinocarbenium Hexafluorophosphate (COMU: 58 g, 368 mmol) were added at 0°C under Ar atmosphere, and stirred for 1 h at room temperature. After cooling to 0°C, *N*-Boc-isoleucine (89.4 g, 341 mmol) was added and stirred overnight at room temperature, and then concentrated *in vacuo*. The residue was diluted with $CHCl_3$ (2 L) and washed with water (1.5 L) twice, concentrated *in vacuo*, and thus **S7** (330 g, *quant*.,

black oil) was obtained. This compound was used in the next step without further purification.

To a solution of **S7** (330 g) in CH_2Cl_2 (1.6 L), trifluoroacetic acid (TFA: 800 mL) was added at room temperature under Ar atmosphere and stirred for 2 h at the same temperature. The resulting solution was concentrated *in vacuo*, and then dissolved in AcOEt (1 L), washed with *sat*. $NaHCO_3$*aq*. (600 mL) twice, dried over Na_2SO_4, filtered, and concentrated *in vacuo*. The residue (315 g) was purified by NH-silica gel column chromatography (2.3 kg, elution with 0-5 % MeOH/$CHCl_3$), and thus **S8** (97.5 g, 76 % yield, yellow solid) was obtained.

To a solution of **S3** (139 g, 285 mmol) in *N*,*N*-dimethylformamide (DMF: 1250 mL), DIPEA (77.1 mL) and 1-[bis(dimethylamino)methylene]-1*H*-1,2,3-triazolo[4,5-*b*]pyridinium 3-oxide hexafluorophosphate (HATU: 109 g, 259 mmol) were added at 0°C under Ar atmosphere. After stirring for 30 min at the same temperature, **S8** (97.4 g, 259 mmol) was added at 0°C and stirred overnight at room temperature. The resulting solution was diluted with AcOEt (2.5 L) and water (1.5 L) and extracted with AcOEt (1.5 L). The

96 combined organic layer was concentrated *in vacuo* and azeotroped with toluene. The

97 residue (448 g) was purified by NH-silica gel (6.0 kg, elution with 0-4 %

98 MeOH/$CHCl_3$) and concentrated *in vacuo*. After dissolving in MeOH (500 mL),

99 insoluble was filtered off and the filtrate was concentrated *in vacuo*. The residue was

100 suspended in Me_2CO (1.5 L), stirred, and cooled to room temperature. Subsequently, a

101 precipitate was collected, and thus **TUS-007** (117 g, 53 % yield, yellow solid) was

102 obtained.**TUS-007**: ^{1}H-NMR (400 MHz, DMSO-d_6) δ 0.83 (3H, d, J = 6.4 Hz),

103 0.74-0.88 (6H, m), 0.87 (3H, d, J = 6.4 Hz), 1.08-1.28 (5H, m), 1.36-1.59 (8H, m),

104 1.75-1.82 (1H, m), 2.07-2.21 (2H, m), 2.94-3.08 (2H, m), 3.81-3.92 (2H, m), 4.22-4.38

105 (4H, m), 6.89-6.93 (1H, m), 7.02-7.06 (1H, m), 7.14-7.44 (4H, m), 7.34 (1H, d, J = 8.2

106 Hz), 7.52 (3H, s), 7.88-7.97 (4H, m), 8.78 (1H, t, J = 5.7 Hz), 9.96 (1H, d, J = 22.4 Hz),

107 10.92 (1H, s), 11.93-11.97 (1H, m). HR-MS (FAB) *m/z*: 845.3674 (Calcd for

108 $C_{44}H_{55}Cl_2N_8O_5$ $[M+H]^+$ 845.3672).

109

110

111 **The synthesis of MDM2-CANDDY.**

112 MDM2-CANDDY was synthesized as shown below. Some of the compounds were

113 synthesized by the NARD Institute. Ltd. (Kobe, Japan).

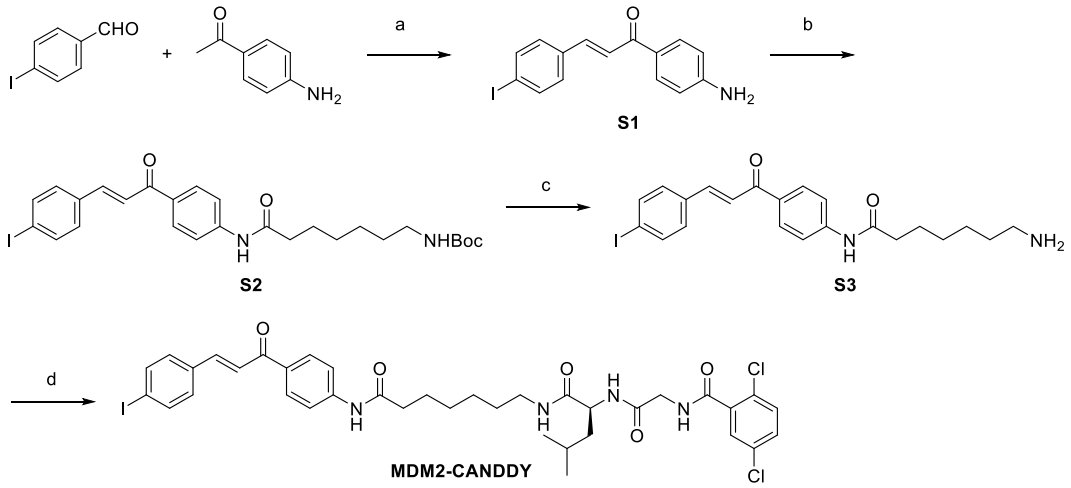

114 Reagent and conditions: (a) 40% KOHaq., EtOH, 0°C to rt, 60%; (b) 7-{(*tert*-Butoxycarbonyl)amino}heptanoic acid, HATU, DIPEA, DMAP, DMA/CH_2Cl_2, 0°C to rt, 70%; (c) TFA, CH_2Cl_2, 0°C, 99%; (d) CANDDY-MLN, HATU, DIPEA, DMF/CH_2Cl_2, 0°C to rt, 65%.

115 To a solution of 4-Iodobenzaldehyde (7.00 g, 30.1 mmol) and 4′-Aminoacetophenone

116 (4.08 g, 30.1 mmol) in EtOH (90 mL), 40% KOH*aq*. (60 mL) was added dropwise over

117 1 h at 0°C and stirred for 1 h under Ar atmosphere. After stirring for 6 h at room

118 temperature, the resulting solution was cooled to 12°C. A precipitate was collected by

119 filtration and washed with EtOH-water (1:2, 80 mL). The collected solid was dissolved

120 in $CHCl_3$ (800 mL) and the insoluble content was filtered and removed. The filtrate was

121 washed with water twice, dried over Na_2SO_4, filtered, concentrated *in vacuo*, and thus

122 **S1** (6.27 g, 60% yield, yellow solid) was obtained. This compound was used without

123 further purification.

124 To a solution of **S1** (6.16 g, 17.7 mmol), 7-{(*tert*-Butoxycarbonyl)amino}heptanoic acid

125 (4.35 g, 17.7 mmol), and DIPEA (4.62 mL, 26.5 mmol) in CH_2Cl_2-*N*,*N*-dimethyl-

126 acetamide (DMA: 10:1, 170 mL), HATU (10.2 g, 26.8 mmol) was added at 0°C under

127 Ar atmosphere. After stirring for 1 h at the same temperature, the solution was warmed

128 to room temperature and stirred for 4 h, and then 4-dimethylaminopyridine (DMAP:

129 250 mg, 2.04 mmol) was added, and stirred further 17 h at ambient temperature. After

130 stirring for 48 h at 30°C, the resulting solution was diluted with CH_2Cl_2 (1.2 L) and

131 washed with water (0.6 L), 1N HClaq. (0.6 L) twice, sat. $NaHCO_3$aq. (0.6 L) and brine

132 (0.6 L). The combined organic layer was dried over Na_2SO_4, filtered, and concentrated

133 in vacuo. The residue was purified by silica gel column chromatography (elution with

134 10-50% AcOEt/heptane). Next, the resulting rough solid was suspended in AcOEt (150

135 mL) at 50°C for 1 h and IPE (300 mL) was added, and the mixture was cooled on

136 ice-bath. A precipitate was collected, and thus **S2** (7.14 g, 70% yield, pale yellow solid)

137 was obtained.

138 To a solution of **S2** (2.50 g, 4.34 mmol) in CH_2Cl_2 (125 mL), TFA (63 mL) was

139 added at 0°C under Ar atmosphere. After stirring 1.5 h at the same temperature, the

140 resulting solution was concentrated *in vacuo*. The residue was dissolved in CH_2Cl_2,

141 poured into sat. $NaHCO_3$aq./water (2:1, 300 mL) and stirred for 1 h. The precipitate was

142 collected by filtration, washed with water (20 mL) twice, dried *in vacuo*, and thus **S3**

143 (2.05g, 99% yield, pale orange solid) was obtained.

144 To a solution of **CANDDY_MLN** (MLN2238 derived CANDDY tag: 0.72 g, 2.0 mmol,

145 synthesized by WO2018092723) in DMF/CH_2Cl_2 (1:1, 20 mL), DIPEA (0.32 mL, 1.9

146 mmol) and HATU (0.76 g, 2.0 mmol) were added at 3°C. After stirring at same

147 temperature for 30 min, **S3** (0.90g, 1.9 mmol) was added and warmed to room

148 temperature, stirred for further 3 h at room temperature. The resulting solution was

149 evaporated, diluted with water (200 mL), and stirred. A precipitate was collected by

150 filtration, dried *in vacuo*, and thus **MDM2-CANDDY** (1.0 g, 65% yield, white solid)

151 was obtained. **MDM2-CANDDY**: ^{1}H-NMR (400 MHz, DMSO-d_6) δ 0.84 (3H, d, J =

152 6.5 Hz), 0.87 (3H, d, J = 6.5 Hz), 1.25-1.31 (4H, m), 1.38-1.46 (4H, m), 1.53-1.59 (3H,

153 m), 2.33 (2H, t, J = 7.2 Hz), 2.97-3.07 (2H, m), 3.81-3.91 (2H, m), 4.25-4.31 (1H, m),

154 7.52 (3H, s), 7.64 (1H, d, J = 15.8 Hz), 7.67 (2H, d, J = 8.5 Hz), 7.76 (2H, d, J = 8.9

155 Hz), 7.82 (2H, d, J = 8.5 Hz), 7.91-7.98 (2H, m), 7.96 (1H, d, J = 15.8 Hz), 8.12 (2H, d,

156 J = 8.9 Hz), 8.78 (1H, dd, J = 5.9, 5.9 Hz), 10.23 (1H, s). HR-MS (FAB) m/z: 819.1577

157 (Calcd for $C_{37}H_{42}Cl_2IN_4O_5$ $[M+H]^+$ 819.1577).

158

Supplementary Figures for **"*In vivo* KRAS G12D/V degradation mediated by CANDDY using a modified proteasome inhibitor"**.

Satoshi Imanishi, Lijuan Huang, Shoko Itakura, Masamichi Ishizaka, Yoichi Iwasaki, Tomohiro Yamaguchi, and Etsuko Miyamoto-Sato

a

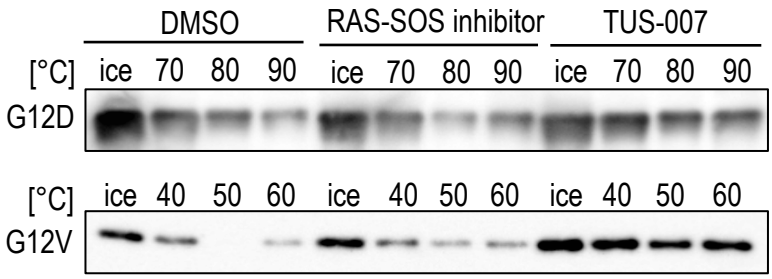

b

	T_m (°C)
DMSO	48.8 ± 0.05
RAS-SOS inhibitor	50.1 ± 0.15*
TUS-007	51.5 ± 0.2*,#

Fig. S1. The heat resistance of KRAS G12D/V incubated with TUS-007.
a, Evaluation of the target-binding affinity of TUS-007 to KRAS mutants by a thermal shift assay. Recombinant KRAS was treated with the vehicle, RAS-SOS inhibitor, or TUS-007 for 30 min, heated at the indicated temperature for 20 min, then analyzed by immunoblotting. **b,** The means of T_m values from fluorescence-based thermal shift assay shown in Fig. 1d. (mean ± SEM; n = 2). *P < 0.05 vs. DMSO, #P < 0.05 vs. RAS-SOS inhibitor.

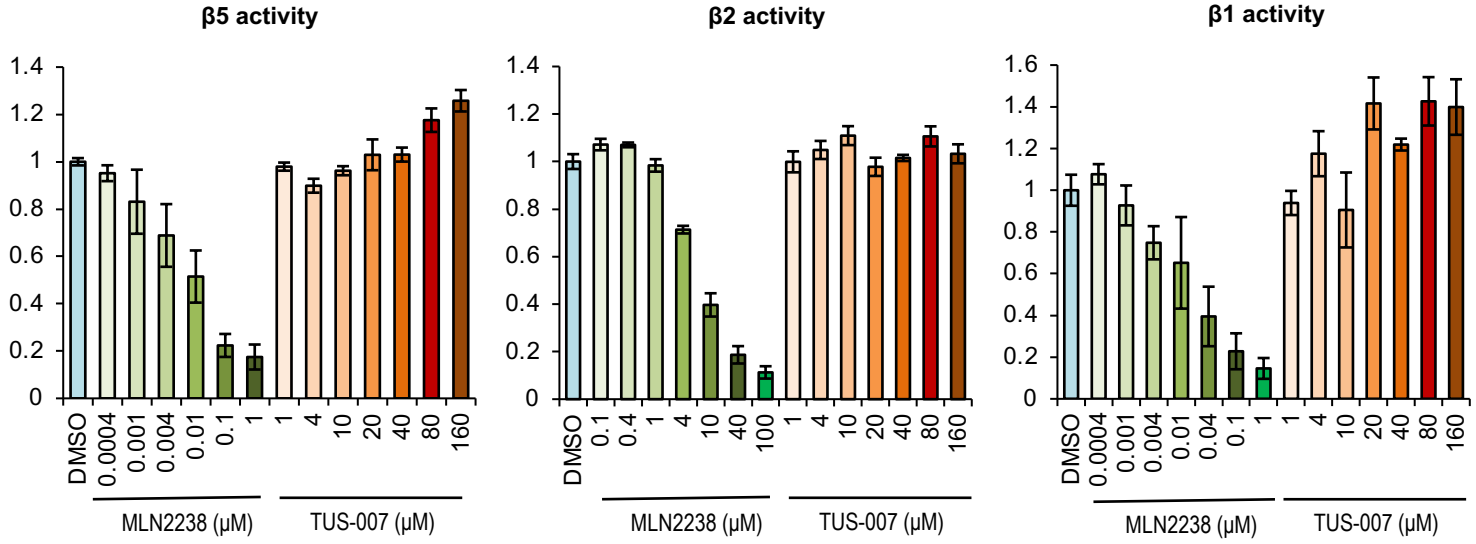

Fig. S2. Effects of TUS-007 on proteasome activity levels.
The levels of chymotrypsin-like (β5), trypsin-like (β2), and caspase-like (β1) proteasome activities was monitored by Suc-LLVY-AMC, Bz-VGR-AMC, and Z-LLE-AMC, respectively. AMC fluorescence was monitored by a plate reader with excitation and emission filters of 360 and 460 nm, respectively (DMSO, 30 min = 1) (mean ± SEM; n = 2–3).

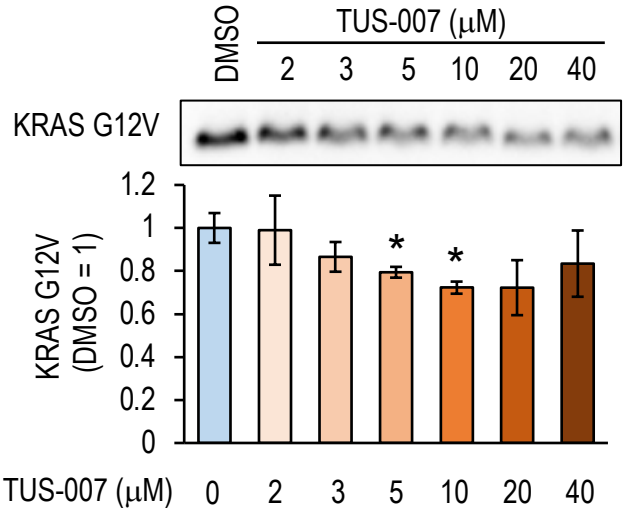

Fig. S3. TUS-007 induced degradation of KRAS G12V in cell free assay.
Successful KRAS G12V degradation by TUS-007. KRAS G12V protein was incubated with TUS-007 at the indicated concentrations in the presence of 26S proteasome for 1 h (mean ± SEM; n = 3). *P < 0.05 vs. DMSO.

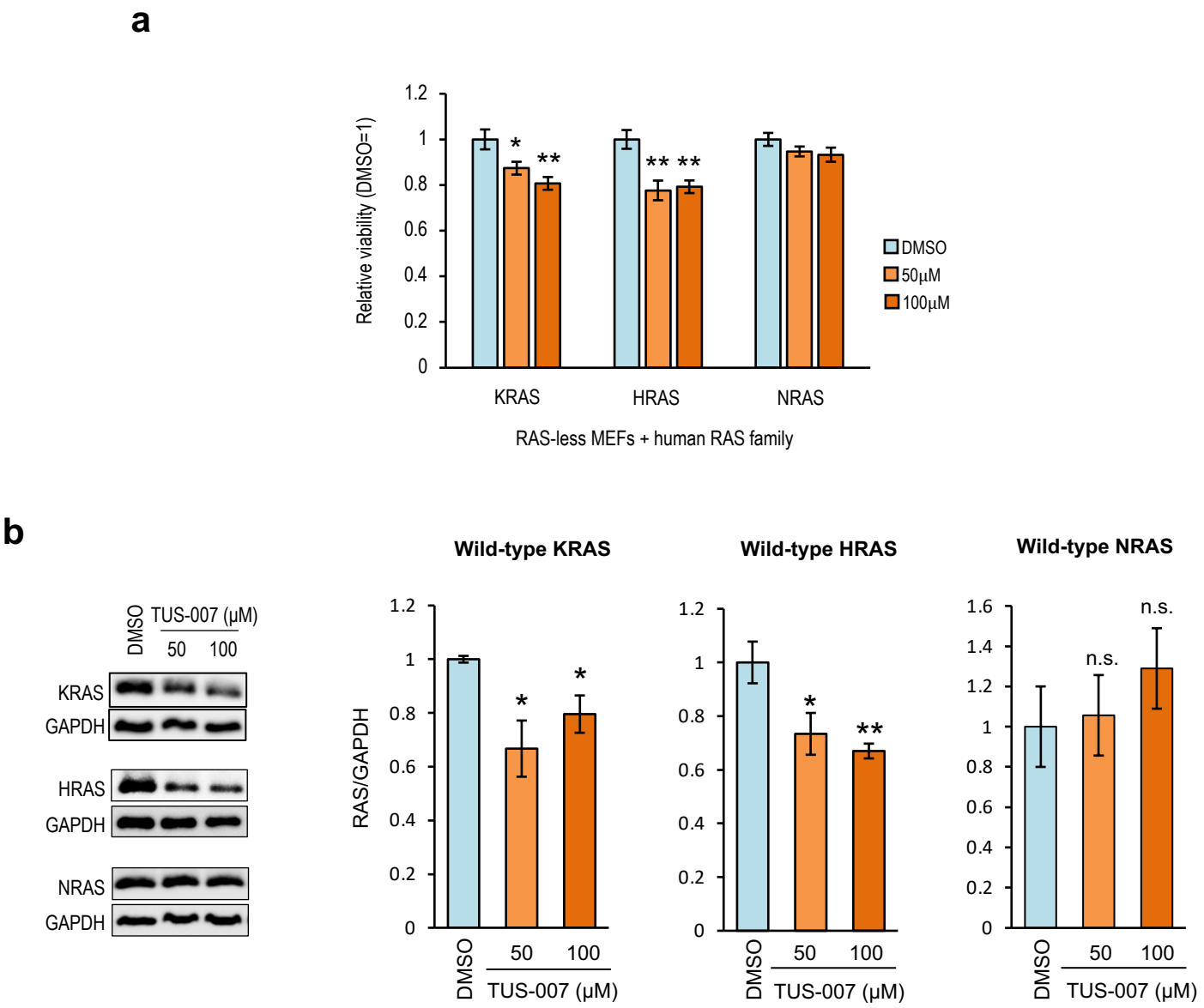

Fig. S4. Selective chemical-knockdown of RAS variants in RAS-less MEFs expressing different types of human RAS. a, Relative viability of RAS-less MEFs expressing WT human RAS family members after incubation with TUS-007 or DMSO. (mean ± SEM; n = 3–5). *P < 0.05 and **P < 0.01 vs. DMSO. **b,** Degradation of WT human RAS family members in RAS-less MEFs treated with TUS-007 or DMSO for 72 h (mean ± SEM; n = 4–5). *P < 0.05 and **P < 0.01 vs. DMSO.

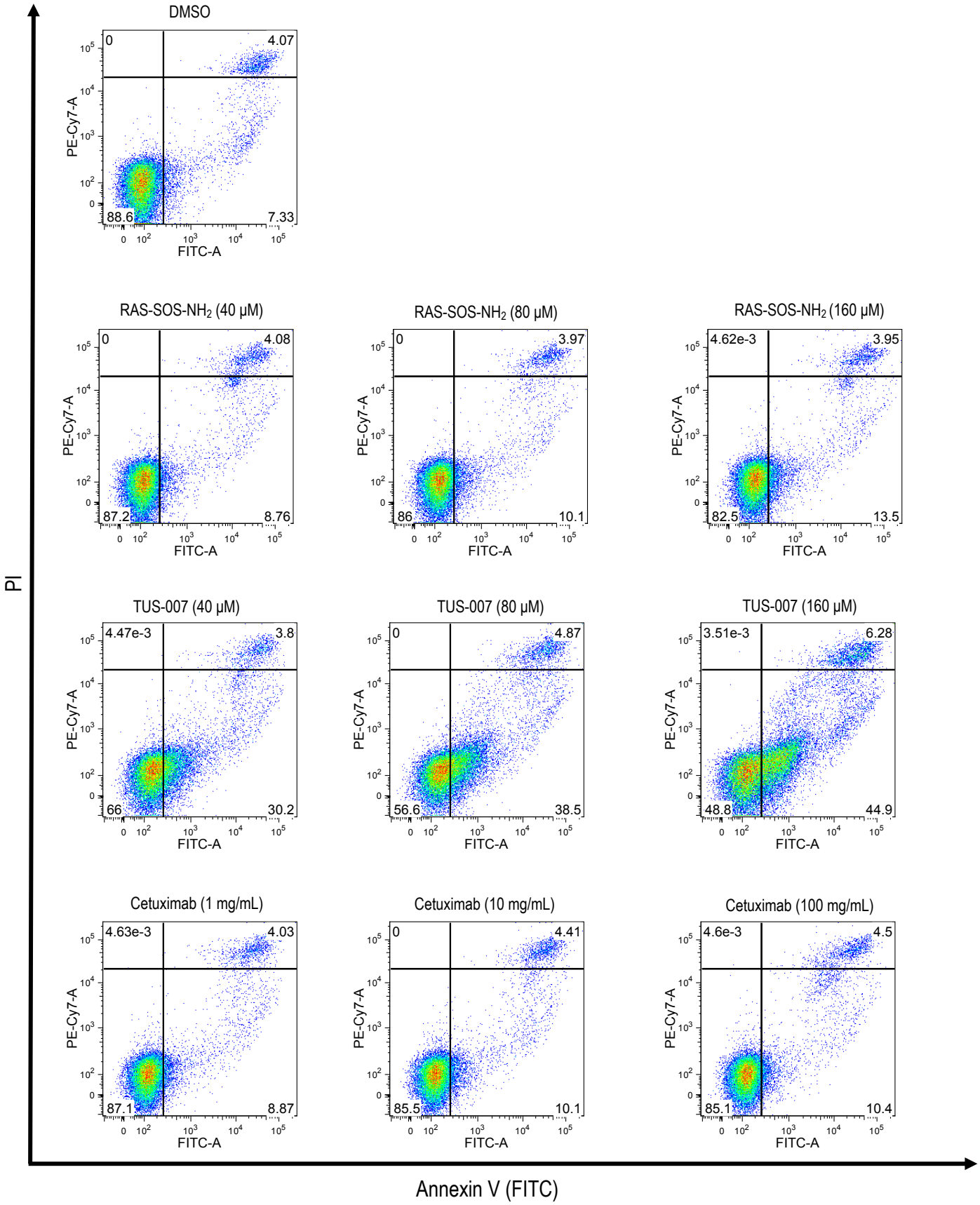

Fig. S5. FACS plots for Annexin V- PI staining of SW620-Luc cells.
SW620-Luc cells were treated with the indicated agents for 48 h, followed by staining with Annexin V-FITC and PI. The typical plots are shown.

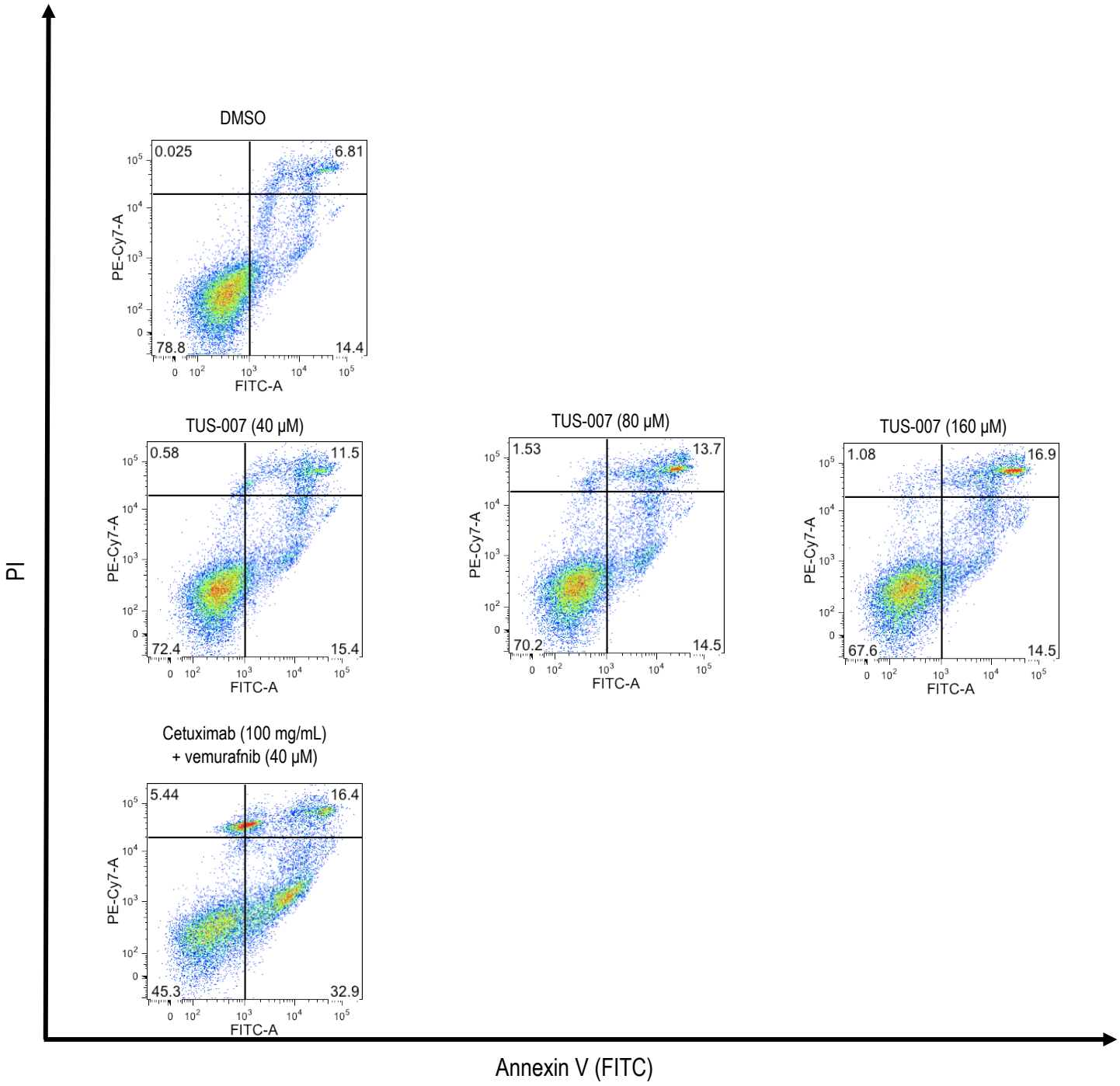

Fig. S6. FACS plots for Annexin V- PI staining of HT29-Luc cells.
HT29-Luc cells were treated with the indicated agents for 48 h, followed by staining with Annexin V-FITC and PI. The typical plots are shown.

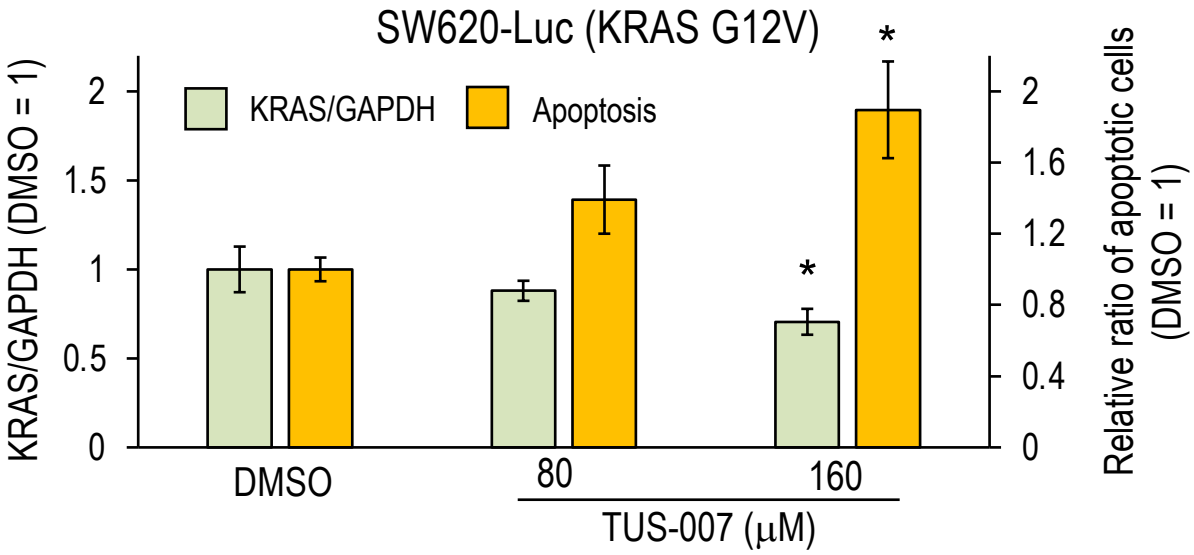

Fig. S7. TUS-007 induced apoptosis only when KRAS degradation was detected in KRAS G12V driven cancer cells. SW620-Luc cell were treated with TUS-007 for 12 h (mean ± SEM; n = 3). The left axis indicates KRAS/GAPDH, and the right axis indicates relative ratio of apoptotic cells. *$P < 0.05$ vs. DMSO. The ratio of KRAS/GAPDH was determined by image analyses of immunoblotting and ration of apoptotic cells were measured using FACS.

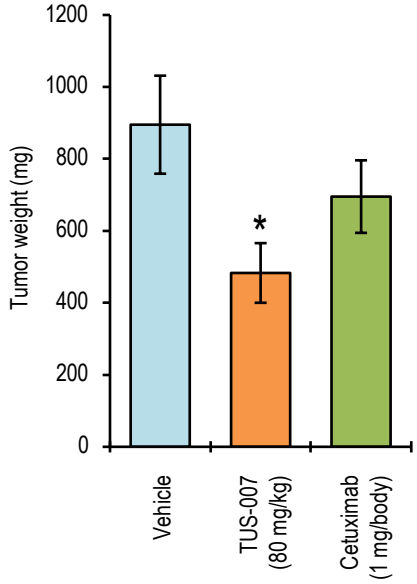

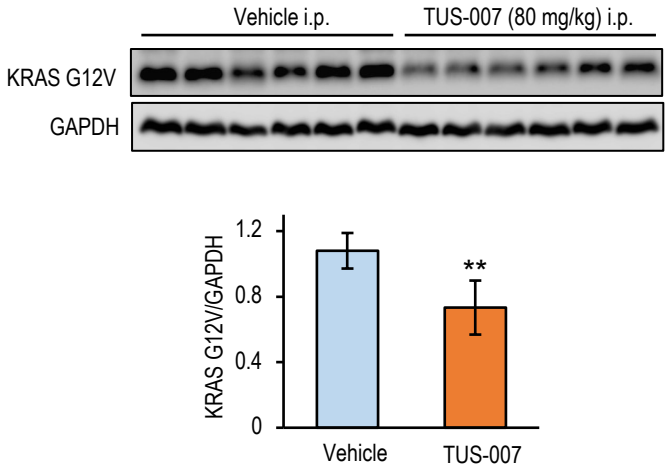

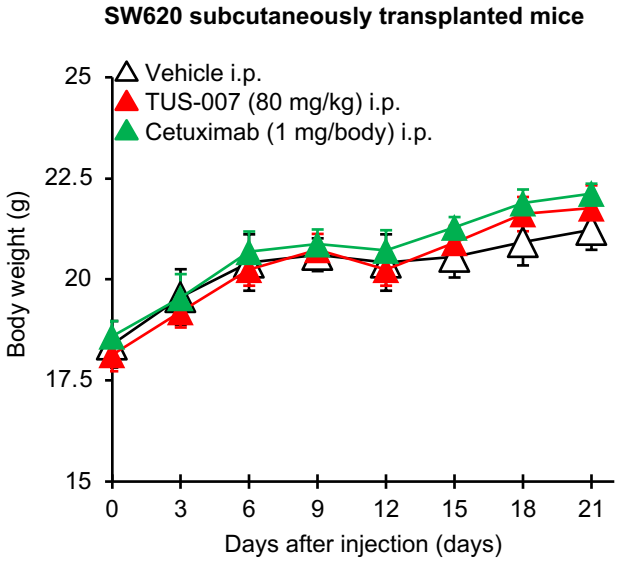

Fig. S8. Effects of TUS-007 on the growth of colon cancer subcutaneous xenografts and toxicity.
a, Comparison of SW620-Luc tumor weight at 21 days after injection (mean ± SEM; n = 6–8). *P < 0.05 vs. vehicle alone. **b,** Immunoblotting of KRAS G12V chemical knockdown in tumors from the same mice used in Fig. 2e (mean ± SEM; n = 6). **P < 0.01 vs. vehicle alone **c,** Body weight changes in mice with SW620-Luc cells transplanted subcutaneously (mean ± SEM; n = 6–8).

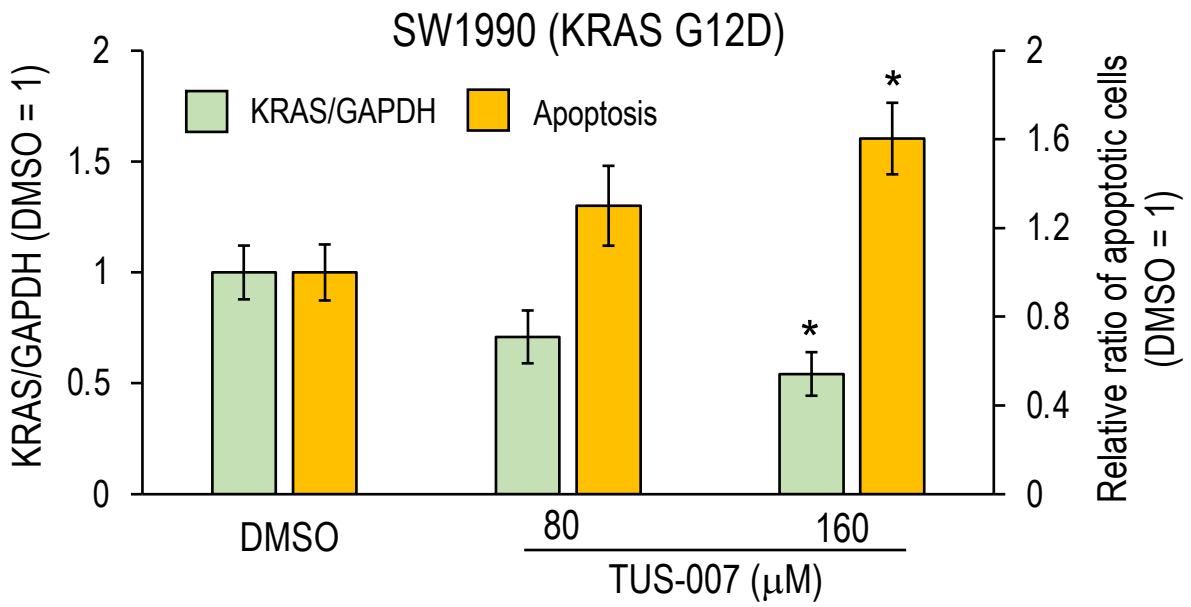

Fig. S9. TUS-007 induced apoptosis only when KRAS degradation was detected in KRAS G12D driven cancer cells. SW1990 cell were treated with TUS-007 for 12 h (mean ± SEM; n = 3).). The left axis indicates KRAS/GAPDH, and the right axis indicates relative ratio of apoptotic cells. *P < 0.05 vs. DMSO. The ratio of KRAS/GAPDH was determined by image analyses of immunoblotting and ration of apoptotic cells were measured using FACS.

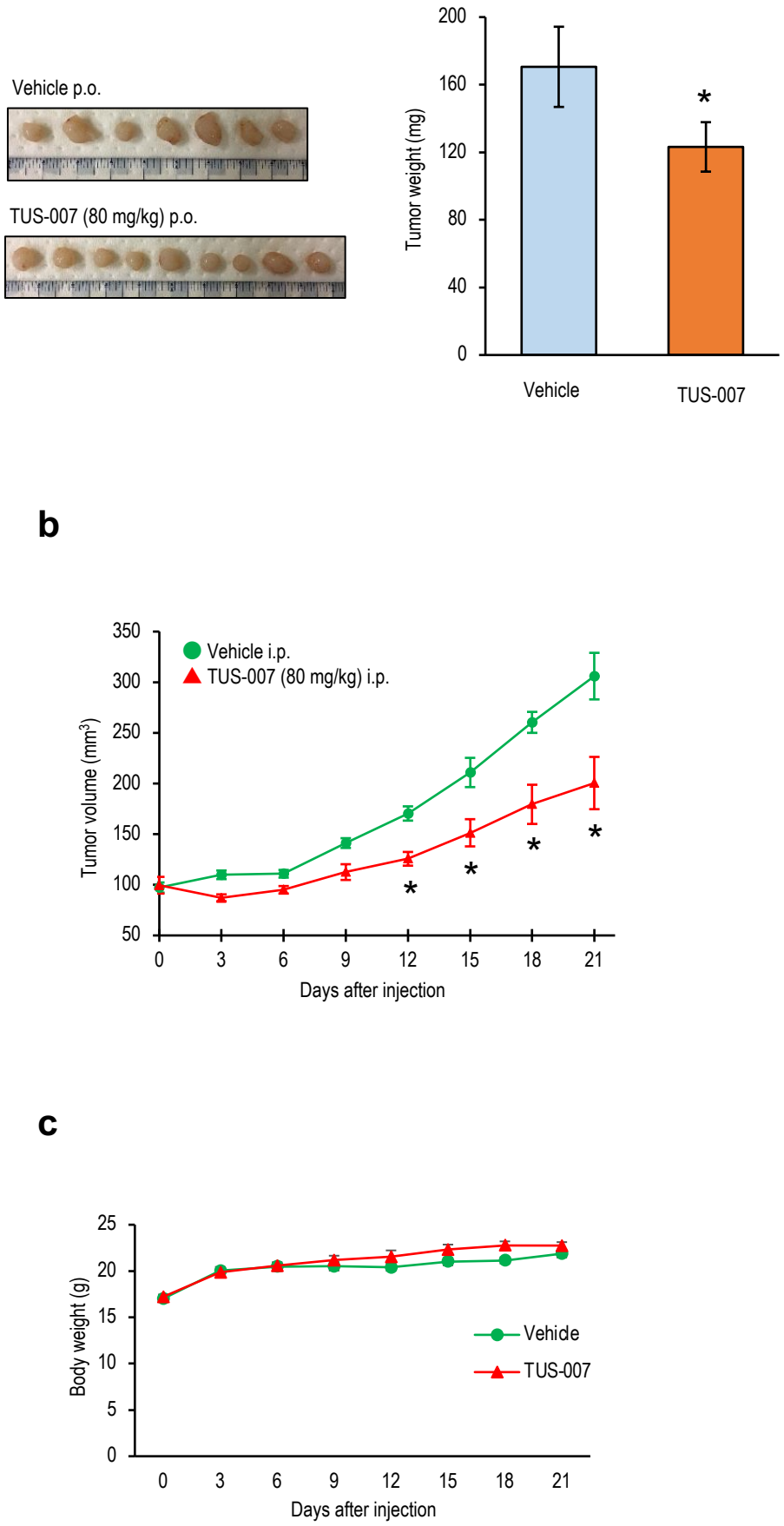

Fig. S10. Effects of TUS-007 on the growth of pancreatic cancer subcutaneous xenografts and toxicity.
a, Tumors of SW1990 cells from the same mice shown and comparison of tumor weight in Fig. 3e at 21 days after p.o. administration (mean ± SEM; n = 6–9). *P < 0.05 vs. vehicle alone. **b,** Tumor volume in mice with SW1990 cells transplanted subcutaneously and treated with i.p. administered TUS-007 or vehicle (mean ± SEM; n = 6–9). The agents were administered every three days. *P < 0.05 vs. vehicle. **c,** Body weight changes in mice with SW1990 cells transplanted subcutaneously (mean ± SEM; n = 6–9).

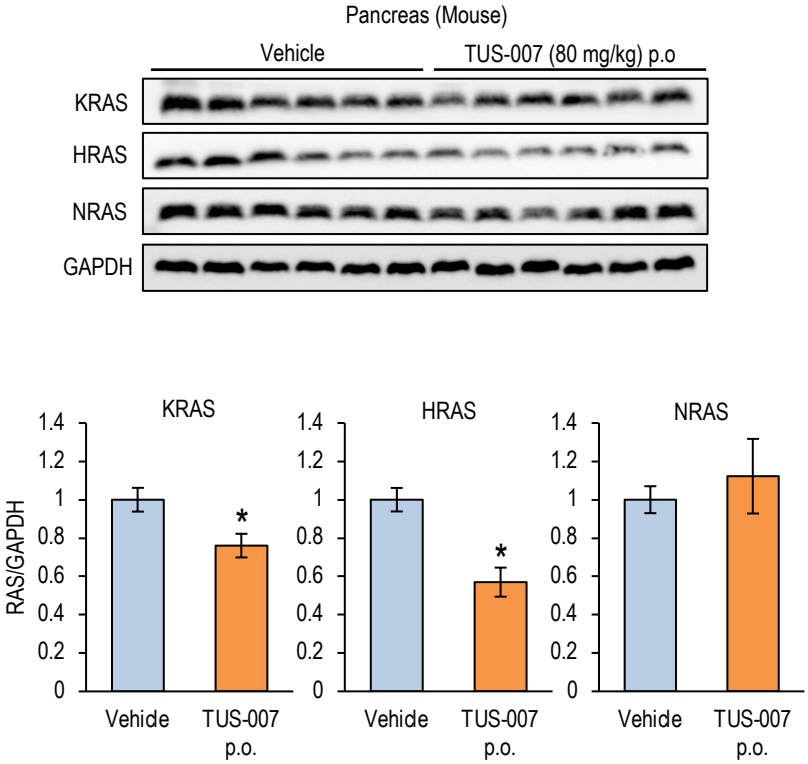

Fig. S11. Effects of oral treatment with TUS-007 on wild type RAS in pancreas.
The immunoblotting analyses of wt RAS proteins in pancreas from the same mice shown in Fig. 3e (mean ± SEM; n = 6–9). *P < 0.05 vs. vehicle alone.

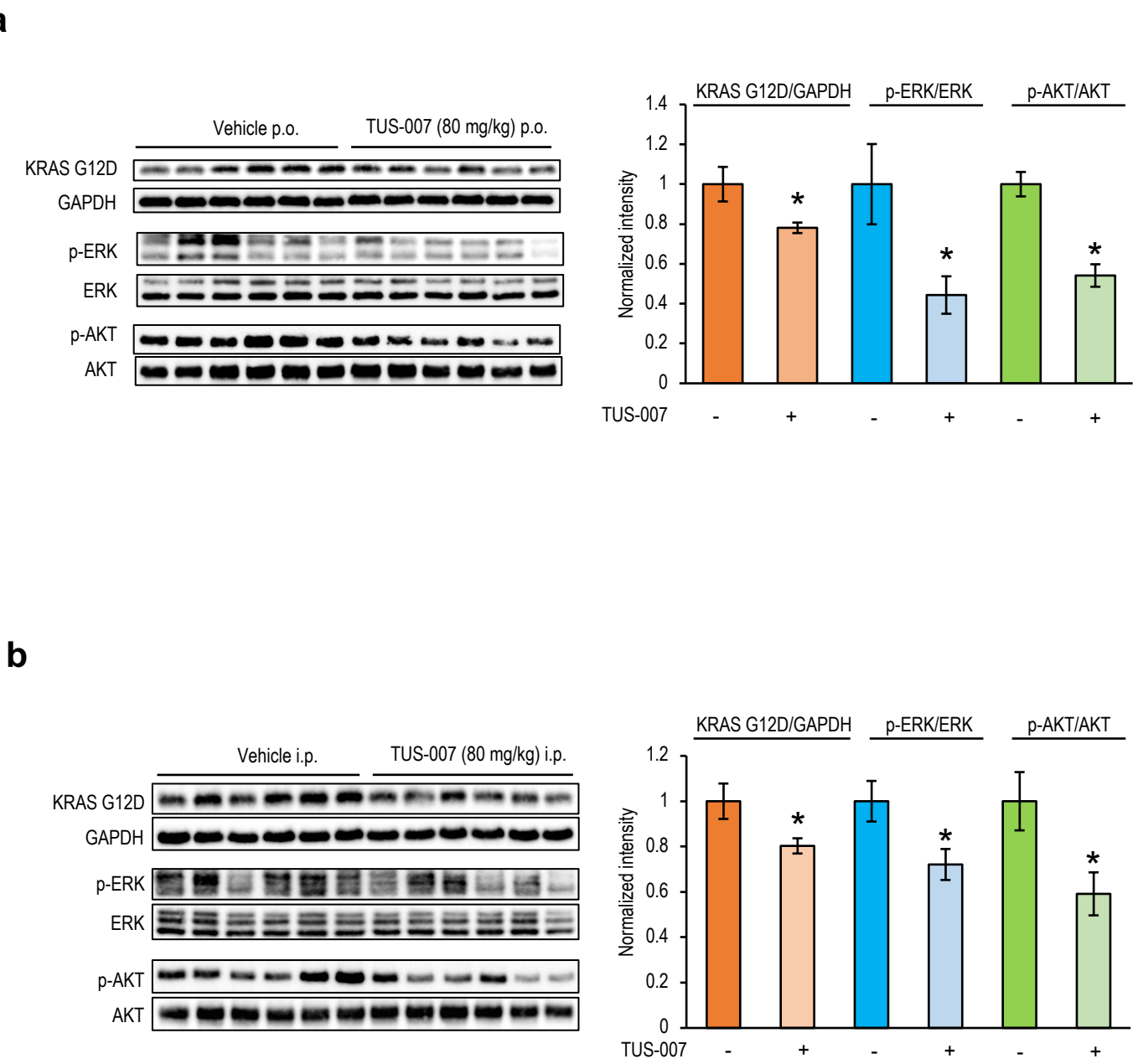

Fig. S12. Effect of of TUS-007 on RAS signaling in pancreatic cancer subcutaneous xenografts. .
Immunoblotting of KRAS and downstream signaling molecules in tumors from the same mice used in Fig 3e (**a**: p.o. treatment) and Supplementary Fig. 11c (**b**: i.p. treatment). The quantitative analysis of the immunoblotting was shown as bar graph, where the KRAS values were normalized to GAPDH, the p-ERK values were normalized to the total ERK, and the p-AKT values were normalized to the total AKT (mean ± SEM; n = 6). *P < 0.05 vs. vehicle.

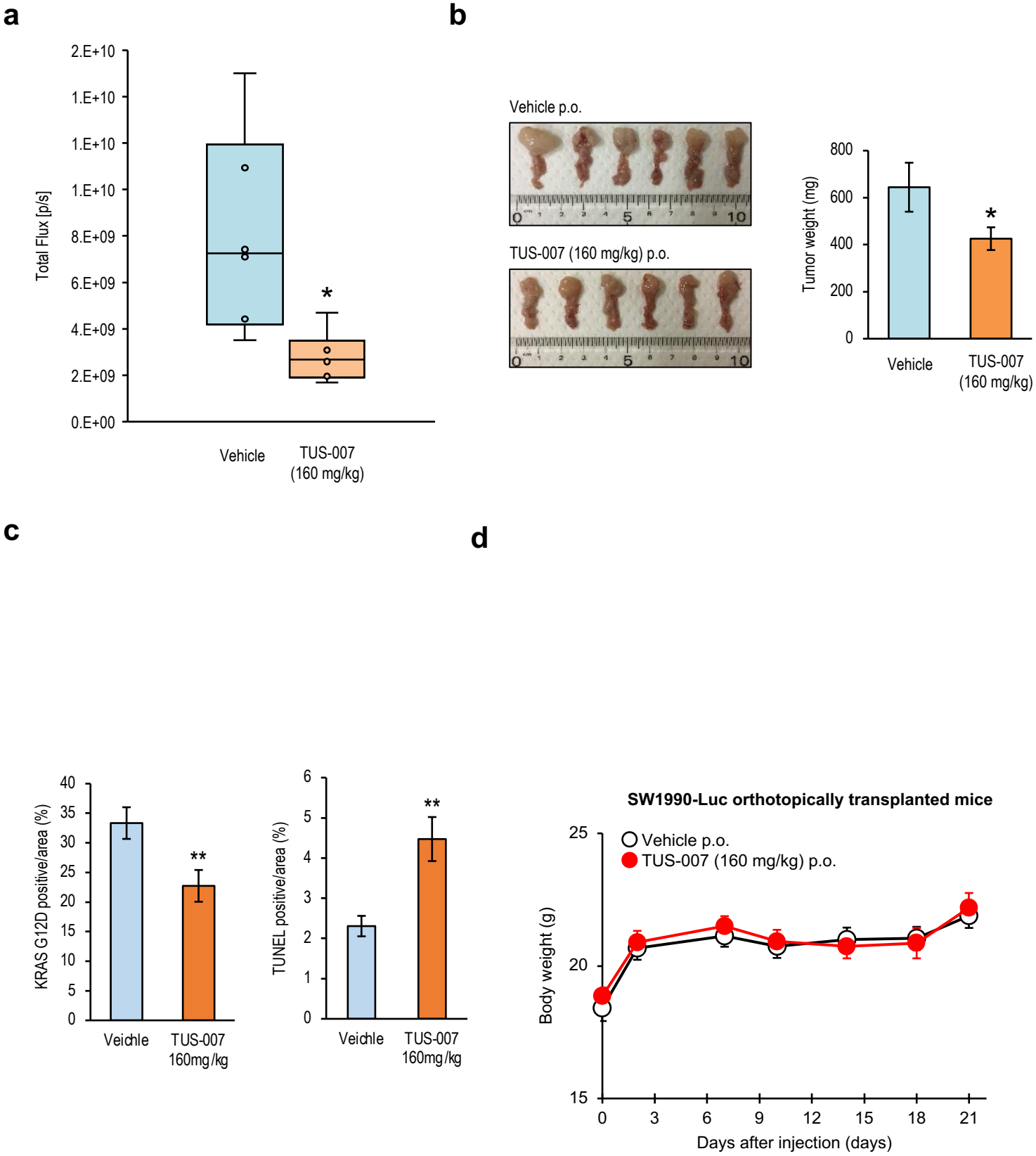

Fig. S13. Effect of TUS-007 on growth of orthotopic pancreatic cancer xenografts expressing mutant KRAS.
a, Tumor growth, as assessed by luciferase signal, in individual mice orthotopically transplanted SW1990-Luc cells treated with TUS-007 (red) or vehicle alone (blue) (mean ± SEM; n = 6). **b,** Pancreases from orthotopic xenograft model mice at day 21 after treatment with TUS-007 (lower-left panel) or the vehicle alone (upper-left panel) and comparison of their weights (right graph) (mean ± SEM; n = 6). *P < 0.05 vs. vehicle alone. **c,** . The quantitative analyses of the KRAS G12D-positive area (left) and TUNEL-positive area (right) in Fig. 4c (mean ± SEM; n = 6). **P < 0.01 vs. vehicle alone. **d**, Body weight changes in mice subjected to orthotopic transplantation of SW1990-Luc cells (mean ± SEM; n = 6).

a

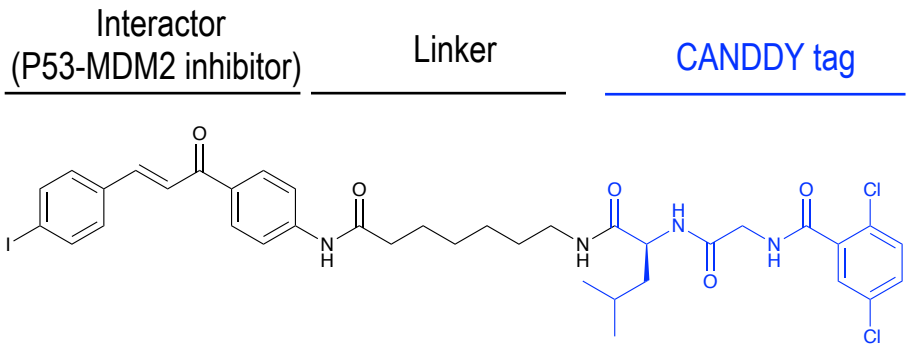

b

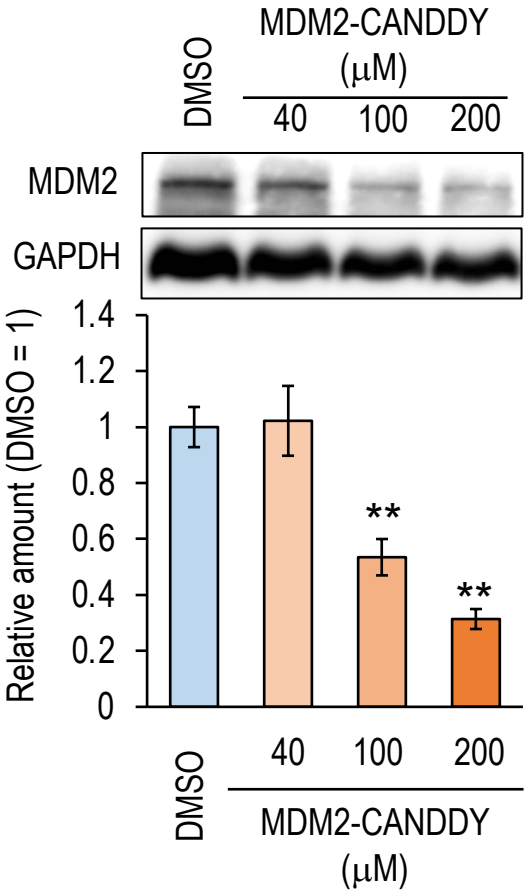

Fig. S14. CANDDY induced degradation of MDM2, a common undruggable target.
a, The structure of MDM2-CANDDY using P53-MDM2 PPI inhibitor, with IC50 value between 6-25 μM. **b,** MDM2-CANDDY degraded MDM2 in the dose dependent manner. The human colon cancer cells HCT-116 were incubated for 48 h with MDM2-CANDDY (mean ± SEM; n = 3). **P < 0.01 vs. DMSO.

Table S1. The concentration of TUS-007 in pancreas was maintained for 72 h.
The concentration of TUS-007 in pancreas from healthy wild-type mice i.p. treated with TUS-007 at 80 mg/kg (means ± SEM; n = 5). The samples were obtained at indicated time points after i.p. injection. The concentration of TUS-007 was measured with HPLC.

Hours after i.p	1h	20h	72h
TUS-007 in pancreas (ng/mg)	45.7 ± 20.3	55.0 ± 28.6	61.8 ± 30.0